Waveform Modeling, Migration and Tomographic Analysis of Seismic Anisotropy

by

Fan Jiang, Ph.D.

A Dissertation
In

GEOSCIENCES

Submitted to the Graduate Faculty
of Texas Tech University in
Partial Fulfillment of
the Requirements for
the Degree of

DOCTOR OF PHILOSOPHY

Approved

Chair: Professor Hua-wei Zhou

Associate Professor Harold Gurrla

Associate Professor Seiichi Nagihara

Fred Hartmeister
Dean of the Graduate School

07. 2010

ACKNOWLEDGMENTS

I wish to express my thanks to all those who have contributed in any way towards the completion of this dissertation:

I am very grateful to my supervisor Professor Hua-wei Zhou for his valuable guidance, fruitful suggestions, encouragement and friendship towards my PhD dissertation accomplishment. The numerous discussions, even arguments, have been a constant source of idea-inspiration.

Special gratitude goes to Professor Nagihara Seiichi and Professor Harold Gurrola for their patient guidance and critical instruction during my dissertation preparation. I would like to thank Dr. Fatmir Hoxha from SeismicCity Inc. and Dr. Shengwen Jin from Halliburton to provide valuable suggestions on my research during my internship.

I would cordially like to thank my colleagues for their frequent discussions and suggestions during my study. A friendly environment in the Department of Geosciences provides excellent and artistic place for my Ph.D. research.

Finally, deepest gratitude to my parents for their continuous encouragement and support for my education and dearest thanks to my wife, Jing-xuan Yu, for her patient during countless evening and weekend which I spend on the research and dissertation.

TABLE OF CONTENTS

ABSTRACT

Seismic anisotropy, the variation of the speed of seismic waves as a function of traveling direction, could be caused by alignments of mineral crystals, fractures, and thin layers of alternative velocities. While most of the current velocity analysis algorithms assume the subsurface be isotropic, in the presence of seismic anisotropy, a proper treatment of seismic anisotropy when it presents will avoid the corresponding error in seismic imageries and provide estimates of the anisotropic structure that might be indicative of lithology and/or the existence of fractures.

In this study, two anisotropic processing algorithms in depth domain are developed to estimate the degree of velocity anisotropy of multi-layer transversely isotropic media with vertical symmetry axis (VTI) or tilted symmetry axis (TTI), and to image the complex subsurface structure. The work primarily involves examining and estimating anisotropic parameters of layered media using first arrival traveltime tomography, and analyzing the influence of anisotropic parameters on the quality of prestack migration. The multi-layered model consists of several thickness-varying layers and the anisotropic parameters are constant for each layer. For each model layer the inversion variables consist of the anisotropic parameters ε and δ, the tilted angle φ of their symmetry axis, layer velocity along the symmetry axes, and thickness variation of the layer. An inversion program was developed to recover several combinations of anisotropic parameters for depth migration.

Inverting for all anisotropic parameters together will make results nonuniqueness, searching for a practical strategy for anisotropic estimation becomes necessary. I evaluate the effects of error in some of the model parameters on the inverted values of the other parameters. The analyses show, for instance, the errors in the layer symmetry axes sensitively affect the inverted values of other parameters, especially δ. However,

the impact of errors in δ on the inversion of other parameters is much less than the impact on δ from the errors in other parameters in crosswell acquisition geometry. Hence, the practical strategy is chosen for different acquisition geometry. In crosswell acquisition geometry, inverting for the most error-tolerant parameters such as layer velocity and ε, and assume constant values for δ. In VSP acquisition geometry, axial velocity and δ could be firstly resolved, when VSP provides large offset, inverting for ε becomes feasible.

By analyzing the anisotropic velocity model, prestack reverse time migration (RTM) algorithm in VTI/TTI media has been applied. RTM propagates the source wavefield forward and receiver wavefield backward in time using acoustic two-way wave equation. RTM has been extended from isotropic media to VTI/TTI media. Explicit finite difference scheme and pseudo-acoustic wave approximation for TI media by simply setting shear velocity as zero are applied for VTI/TTI RTM. By analyzing the effects of each anisotropic parameter on the imaging result of reverse time migration, the importance of each anisotropic parameter for seismic migration is discussed.

LIST OF TABLES

LIST OF FIGURES

CHAPTER 1: INTRODUCTION

1.1 HISTORY OF SEISMIC ANISOTROPY

Seismic anisotropy, the variation of the speed of seismic waves as a function of traveling direction, could be caused by alignments of mineral crystals, fractures, and thin layers of alternative velocities (Figure 1-1). Most of the current velocity analysis algorithms assume the subsurface be isotropic. This assumption greatly simplifies the mathematical treatments and is acceptable for most applications. However, anisotropy of physical properties is part of nature. In the presence of significant level of seismic anisotropy, a proper treatment of seismic anisotropy will be necessary in seismic imaging and estimating the anisotropic structure that might be indicative of lithology and/or the existence of fractures.

Figure 1-1: Alternative thin layers may result in anisotropic structure.

Laboratory studies of rock samples show that many mineral exhibits anisotropic elastic properties, such as Olivine (Figure 1-2). Olivine is a major constituent of the Earth's upper mantle. It contributes more than half of the upper mantle materials.

Olivine material can has large anisotropic effect up to 25% of compressional wave velocity anisotropy. The foliated rocks, such as gneisses, in which mineral alignments have been produced by the metamorphic effects of pressure and temperature, are also expressed as anisotropic property. Another possibility of forming anisotropy is that shape-induced anisotropy at large wavelengths for layered media or distribution of cracks with a preferred orientation, or layered-induced anisotropy.
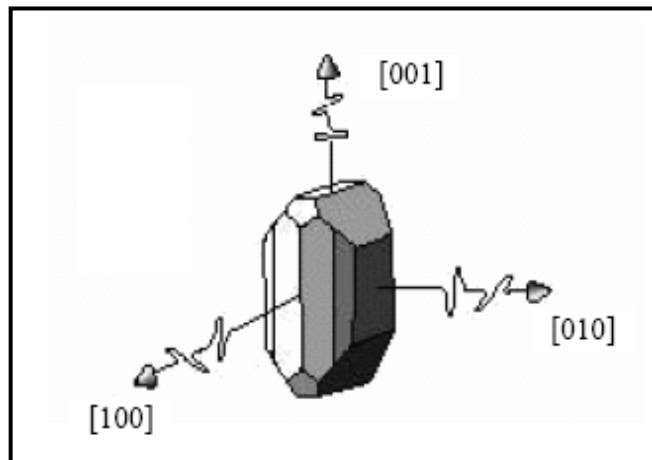
Figure 1-2: Olivine displays anisotropic effect intrinsically. (Zhou, class notes)

However, direct evidence of seismic anisotropy is indeed difficult to observe. Observations from different types of seismic wave sampling the Earth's interior from the crust to the inner core. The elastic anisotropy as observed by seismic wave is different with the intrinsic anisotropy observed in a pure mineral during laboratory experiment. The term, seismic anisotropy, is used to illustrate for anisotropic properties on the scale of wavelength, as opposed to microscopic anisotropy which related to the individual crystals or rock samples. The hidden anisotropy in the Earth may be important when fine details of the Earth's structure need to be investigated, such as targeting the reservoir location. In terms of exploration seismology, without considering anisotropy, it will result in erroneous imaging of subsurface strata, and the reflection point could be imaged away from its true location.

Therefore, many situations which significant anisotropy occurs need to be attempt to understand and treat it mathematically are increasingly common. When sedimentation and tectonic processes produce dip and thickness variations in rock layers, the velocity structures is approximated as the tilted transverse isotropy, or TTI media. For sedimentary strata with a short depositional history the symmetry axis is assumed to be vertical, and for old strata that have undergone deformation the symmetry axes trend to be normal to bedding (*e.g.*: Hornby et al., 1994; Sayers, 2005). In thrust belts like that in the Canadian foothills (Charles et al., 2008), reservoirs are overlain by thick sequences of dipping sandstone and shale layers which generate a tilted symmetry axis which varies with the layer geometry. The tilted angle of the symmetry axis makes it more challenging to estimate the model parameters for the TTI media than that for the VTI (vertical transverse isotropy) media or the HTI (horizontal transverse isotropy) media (Figure 1-3).
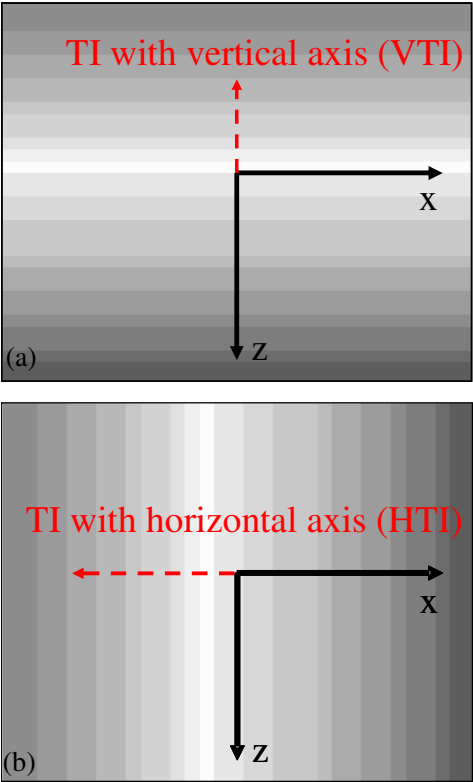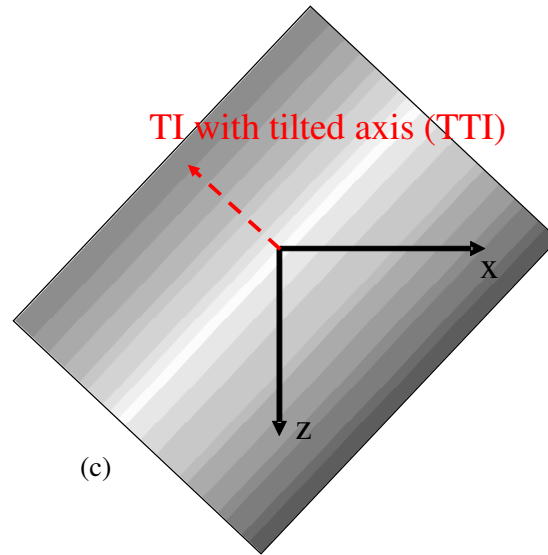
Figure 1-3: Three different types of anisotropic structure. (a) VTI media; (b) HTI media; (c) TTI media.

Explicit estimations of velocity anisotropy are not commonly incorporated into seismic imaging process, largely due to the difficulty in estimating the orientation and magnitude of the anisotropy in depth models. However, parameter estimation in transversely isotropic media has attracted considerable attention in recent years, mostly in time domain analysis by surface reflection data (Alkhalifah and Tsvankin, 1995). A common approach is based on non-hyperbolic NMO type analysis. The layer stripping process using the Dix formula has been shown as a feasible tool for time domain anisotropic analysis (Alkhalifah and Tsvankin, 1995). For a transverse isotropic model with vertical axis, the P-wave velocity is controlled by the axial velocity V_{p0} and the anisotropic parameters ε and δ (Thomsen, 1986). Alkhalifah and Tsvankin (1995) illustrated that only two parameters, the NMO velocity from a horizontal reflector and the anellipticity coefficient η, can be used for anisotropic analysis if the medium above the reflector is laterally homogeneous. Hence, semblance has been considered as an effective tool to define stacking velocity (Alkhalifah, 1997). The semblance coefficient is defined as the ratio of the output energy over a window of a stack of traces to the input energy in the unstacked traces.

Estimating the semblance velocity is based on summing data over hyperbolic trajectories controlled by the trial moveout velocity. Kumar (2008) proposed a common-focus point domain analysis for anisotropic parameter estimation. In this domain, errors in imaging are seen as non-zero differential time shifts, the estimate of anisotropic parameters ε and δ is obtained using least-square solutions of Newton's equation that make the differential time shifts zero.

One of the conclusions that can be drawn from the literature is that in building models in depth domain surface reflection P-wave data are insufficient to constrain the anisotropic velocity and the reflector depth. One reason is that time domain processes are based on layer stripping approach with the Dix formula. It will result in instability due to the accumulation of errors during the procedure. It is still a bottleneck to reconstruct anisotropic models in depth domain for prestack migration using the time domain analyses. On the other hand, seismic tomography is a promising approach to estimate the distributions of anisotropic parameters in depth domain (Chapman and Pratt, 1992). Watanabe et al. (1996) presented a seismic traveltime tomography approach to estimate anisotropic slowness and orientation simultaneously in anisotropic heterogeneous media. Kumar et al. (2004) proposed a ray-based method to calculate TTI traveltime that relies on the computations of group velocity from neighboring eight points. Zhou et al. (2008) proposed a nonlinear kinematic inversion method for crosswell seismic tomography in composite transversely isotropic media with known dipping symmetry axis. Charles et al. (2008) evaluated how velocity and anisotropy mode-building strategies affect seismic imaging in the Canadian Foothills by comparing the results of a model-driven approach with a data-driven approach. Some studies showed that fault plane reflection energy that intersects sedimentary reflectors may be helpful to estimate anisotropic parameters (Ball, 1995). However, these studies show that reliable estimates of layered anisotropic parameters in model space are difficult even when the tilted symmetry axis is known. To reliably estimate δ, for instance, the well control is needed. Large offsets are required to extract ε. A major

challenge is to determine the depth variation of velocity interfaces and anisotropy-induced discrepancy together, especially if only first arrivals are available. Simplifications like models with planar interface or fixed interface geometry have been implemented to constrain the inversion processes.

Considering the varying ability to invert for different model parameters, in this dissertation, I search for ways to invert only for some of the variables in such layered TTI models while fixing the other variables using their default values. By applying the layered tomography method to a series of simple synthetic models, we analyze the impacts of errors in some of the model parameters on the sensitivities of the other parameters. Several experiments suggest that in crosswell acquisition geometry, axial velocity and ε should be considered for priority inversion variables, and consider δ as further inversion parameter when data coverage is sufficient. However, in VSP acquisition geometry, because most raypaths spread around 45°, δ can be considered as priority inversion parameter as well as axial velocity.

Depth domain anisotropic processing can be divided into two categories: The Estimation of Anisotropic Parameters and Anisotropic Depth Migration. In this study, Deformable Layer Tomography (Zhou, 2006) has been extended to consider anisotropy effect using first arrivals. The new anisotropic traveltime tomography can construct the five important anisotropic parameters in depth model: the anisotropic parameters ε and δ, the tilted angle φ of the symmetry axis, layer velocity along the symmetry axis, and thickness variation of the layer. Each anisotropic parameter expresses the presence of velocity variation and can investigate the property of subsurface strata. However, inverting for all anisotropic parameters together will result in nonuniqueness and underdeterminacy to make result unstable. To address those challenges, a practice strategy has been developed with the evaluation the effects of error in some of the model parameters on the inverted values of the other parameters. The analyses show, for example, that the error in the layer symmetry axis significantly

degrades the inverted values of other parameters, especially on δ. However, the impact of the error in δ on the inversion of other parameters is much less than the impact on δ from the error in other parameters. Hence, a practical strategy is first to invert for the most error-tolerant parameters such as layer velocity and ε, and assume zero values for δ. More model parameters can be included in further inversions if they can be resolved by the given data coverage. δ should be the last inversion parameter to be considered in the anisotropic velocity model building.

Anisotropic tomography can provide accurate velocity model, which is required for depth migration. Reverse time migration (RTM) has been successfully applied to produce high-quality images in recent years. It propagates source wavefield forward in time and the receiver wavefield backward to image the subsurface reflector (*e.g.*, Baysal et al, 1983; McMechan, 1983; Whitmore, 1983). By using the two-way acoustic wave equation, RTM has no dip limitation. Also, it naturally takes into account both down-going and up-going waves and thus enables imaging of the turning waves and prism waves that are able to enhance the image of steep salt flank and other steeply dipping events with complex structures. In this dissertation, the influence of different anisotropic parameters on RTM image is analyzed and discussed.

1.2 SUMMARY OF DISSERTATION

Chapter 2 introduces forward modeling algorithms in layered TTI media. Two different forward modeling approaches have been discussed: anisotropic ray tracing and anisotropic finite difference modeling. In the parameter setup of anisotropic ray tracing, each thickness-varying layer consists of constant anisotropic parameter ε and δ, axial velocity and tilted angle of symmetry axis. To compare with the accuracy of anisotropic ray tracing, a pseudo acoustic two-way wave equation is applied to generate waveform data and first arrivals. The application of finite difference, pseudo-

spectral, and hybrid algorithms can be applied to solve the equations. However, the experiments indicates that only finite difference give less computation cost than others and should be considered as default propagator for waveform modeling. The first arrival comparison between anisotropic ray tracing and waveform modeling shows that anisotropic ray tracing can generate good quality of traveltime data as good as waveform modeling, but less computation time. It can be considered as preferred forward modeling algorithm for traveltime tomography.

Chapter 3 introduces P-wave traveltime tomography in layered TTI media. After generating TTI kernels by anisotropic traveltime equation, the inversion scheme can be extended from isotropic to anisotropic approach. Several 2D and 3D numerical experiments show the feasibility of anisotropic layered tomography and illustrate that several combinations of anisotropic parameters indeed can be inverted even traveltime data containing 5% Gauss noise.

Chapter 4 discusses an error analysis of each model parameters on other parameters in terms of inversion quality. Considering the varying ability to invert for different model parameters, searching for ways to invert only for some of the variables in such layered TTI models is needed while fixing the other variables using their default values. By applying the new tomography method to a series of simple synthetic models, the analysis describes the impacts of error in some of the model parameters on the inversion quality of the other parameters. This has led to a strategy to first invert for layer velocity and ε, and to consider δ as the last inversion parameter only when data coverage is sufficient.

Chapter 5 analyzes the imaging errors by different assumptions of anisotropic parameters on the image quality of reverse time migration. Anisotropic parameter ε represents the velocity differences between horizontal direction and vertical direction,

ignoring it will simplify anisotropic media as pseudo-isotropic media. The quality of images will be significantly degraded when ignoring ε. Parameter δ represents that how much wave propagation deviates from vertical direction. The experiments show that δ brings less influence on migration results than ε. The tilted symmetry axis controls the fast direction of wave propagations, ignoring tilted angle will result in errors of the depth and dipping angle of subsurface strata, especially on steeply dipping reflector.

Chapter 6 concludes the innovation and creativity of this dissertation that an anisotropic layered traveltime tomography is developed for velocity model building and the effect of different anisotropic parameters on the images by reverse time migration

CHAPTER 2: FORWARD MODELING IN VTI/TTI MEDIA

2.1 INTRODUCTION

The propagation of seismic body waves in complex anisotropic structures is a complicated process. The common approaches can be investigated by methods based on approximation of high-frequency asymptotic methods, such as ray approach, or direct numerical solution of wave equation, such as finite difference method. Both methods have their own advantages and disadvantages, based on different objectives, a proper method need to be chosen to collaborate with future application.

To calculate raypath traveltime in anisotropic media, ray tracing has been shown as an efficient approach (*e.g.*: Cerveny, 1972; Klimes and Kvasnicka, 1994; Zhou and Greenhalgh, 2005). There are two traditional methods to computer seismic raypaths between two local points: shooting and bending (Cerveny, 2001). The shooting method is based on iterative application of an initial value ray tracing algorithm. This method tries to find raypaths leaving one source point by solving the differential equations until the trial ray arrives at the predefined point. Rays are specified uniquely by the ray take-off parameters. The drawbacks of this method are its convergence problem, especially in 3D area, and can not find ray diffracted raypaths in shadow zones where ray theory breaks down. Another method, bending method, considers Fermat's principle as a starting point. It tries to find a ray path between two points by searching the minimum traveltime between them. Bending method can generate the traveltime of diffracted ray, even when the destination point is in velocity shadow zone. However, bending method is good only for one source-receiver pair at a time

and it is not certain whether the path has an absolute minimal traveltime or only a local minimal traveltime (Moser, 1992).

By applying network theory and shortest paths in networks after Nakanishi and Yamaguchi (1986), Moser (1991) proposed a new ray tracing method to avoid the disadvantages of shooting and bending. Moser's method, named shortest path method, is good to construct all shortest paths from one point at same time. It can be applied to the simulation of common-shot point gathers without missing any receivers in a complex geological structure.

To encounter seismic anisotropy in the propagation of seismic waves, great achievements have been made in theoretical analysis and numerical modeling. Cerveny and Firbas (1984) demonstrated a linearized approach to traveltime computation for a general anisotropic medium. The linearization procedure can be applied to inhomogeneous, slightly anisotropic media to solve direct and inverse kinematic problems. Shearer and Chapman (1988) gave the solutions of the raypath and traveltime in a linear gradient anisotropic medium. Their method can approach the kinematic property of a cell in general anisotropic media by using a target-shooting scheme, which traces a ray with a trial of the phase slowness direction.

Recently, many researchers are interested in anisotropic ray tracing but focusing on VTI media for two reasons. The first reason is that VTI is a good simplification of the structure of minerals in sedimentary rock such as shale to the hexagonal crystals. Some ordering in the structure of rocks, such as fine-layering and parallel cracked, has similar properties with VTI medium (Crampin, 1984). The second reason is that VTI medium provides simplification of mathematical calculation for wave propagation. Ruger and Alkhalifah (1996) developed an efficient 2D ray tracing algorithm based on the simplified version of the eigenvectors in a VTI medium. Cardarelli and Cerreto

(2002) proposed a ray tracing method in elliptical anisotropic media by the interpolation of linear traveltime. To improve the efficiency of Moser's shortest path ray tracing method in anisotropic medium, Zhou and Greenhalgh (2005) proposed a method for seismic ray tracing by extending Moser's SPM in a general anisotropic medium. They showed that the anisotropy may be defined by up to 21 density-normalized elastic moduli which vary with spatial position. They apply analytical solutions of the wave velocities for a general anisotropic medium as a "transform" or "mapping" operator to convert the elastic-moduli-described medium into the direction-dependent group-velocity models for the three independent wave modes (qP, qSV, qSH).

Alternatively, anisotropic acoustic waveform modeling has become a popular way to calculate traveltime and default forward modeling for seismic migration. The primary drawback of the elastic assumption about the Earth's subsurface is that it ignores the inelastic nature of the earth. Elastic assumption also requires the dynamic computation of all three components of the wavefield, resulting in an expensive computational process. To reduce the computation cost, the media with acoustic assumption is used to simulate only P-wave propagation. The wavefield in the acoustic media can be described by a scalar factor other than a vector. The main difference between elastic and acoustic medium is that in elastic medium, the P-wave energy will transform to S-wave energy when encountering an interface but in acoustic medium, all the P-wave energy is conserved.

The acoustic wave equation can be used for zero-offset and nonzero-offset modeling of P-waves. There is no need to separate P-wave and S-wave which can save much computational time. Alkhalifah (1998, 2000) started from dispersion relation and proposed a pseudo-acoustic approximation wave equation in TI media by setting shear wave velocity along the symmetry axis as zero. Based on Alkhalifah's pseudo-acoustic

approximation, a number of variations of pseudo-acoustic wave equation have been developed to account for the vertical TI (VTI) media (Zhou et al., 2006a; Hestholm, 2007; Du et al., 2008). Assuming the symmetry axis is normal to the bedding and tilting the symmetry axis accordingly, extensions from VTI to TTI have been developed (Zhou et al., 2006b; Fletcher et al., 2009; Zhang and Zhang, 2009).

In this chapter, by extending Sena's (1991) anisotropic traveltime equation to TTI media and compared with anisotropic waveform modeling in terms of picked first arrivals, shortest path ray tracing can be proved as effective approach for calculating traveltime data in 2D/3D TTI media. The calculated fist arrivals from ray tracing can be used for traveltime tomography for anisotropic parameter estimations.

2.2 METHODOLOGY OF ANISOTROPIC FORWARD MODELING

2.2.1 Traveltime equation in VTI/TTI media

A basic feature of wave propagation in anisotropic media is that the propagated direction of the ray velocity generally differs from that of the wave-front velocity, or phase velocity (Figure 1). The wavefront is perpendicular to the propagation vector k because the direction of the propagation of the phase is along the vector k. Apparently the wave-front is non-spherical. It is different from ray angle θ which is the angle from the source point to the wavefront. In the other way, the group (ray) velocity is determined by the velocity of energy propagation. In inhomogeneous transversely isotropic media, the group velocity is used to determine the ray angle that the raypath will travel (Slawinski et al., 2000).

13
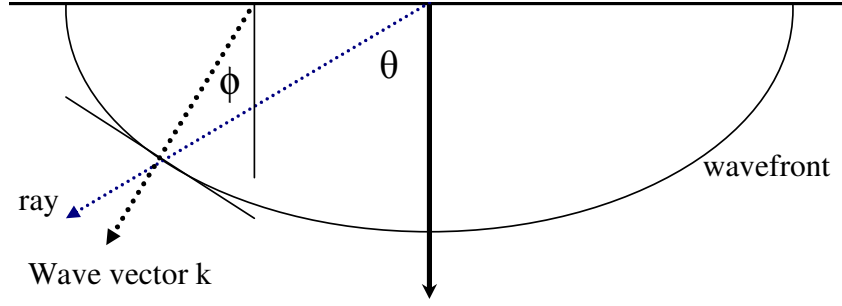
Figure 2-1: Phase angle (ϕ) and group angle (θ).

To determine the phase velocity as well as group velocity, many researchers derived anisotropic traveltime equation based on different assumptions. Expression for the P-wave phase velocity has been obtained by Thomsen (1986) under the weak anisotropy approximation:

$$V_p(\phi) = V_p(0)\left(1 + \delta\sin^2\phi\cos^2\phi + \varepsilon\sin^4\phi\right) \tag{2-1}$$

Where $V_p(\phi)$ is phase velocity at incident angle ϕ, $V_p(0)$ is vertical velocity, ε and δ are anisotropic parameters.

The above equation is obtained by extending the exact expressions of the phase velocity in a Taylor series in the small parameters ε and δ at fixed ϕ, retaining only linear terms in small parameters. The group velocity expression, $V_g(\theta)$, is obtained from Thomsen's derivation (Thomsen, 1986):

$$V_g^2(\theta) = V_p^2(\phi) + \left(\frac{dV_p(\phi)}{d\phi}\right)^2 \tag{2-2}$$

Where θ is the ray angle from the source point to the wavefront (Figure 1). Under weak anisotropy approximation, the relationship between ray angle θ and phase angle ϕ of P wave is given by (Thomsen, 1986):

$$\tan\theta = \tan\phi\left(1 + 2\delta + 4(\varepsilon - \delta)\sin^2\phi\right) \tag{2-3}$$

Substituting Equation (2-2) and (2-3) into (2-1) retaining only linear terms in the small parameters ε, δ and θ shown on Equation (2-4) (Sena, 1991):

$$V_g^{-2}(\theta) = V_g^{-2}(0)(1 - 2\delta\sin^2\theta + 2(\delta-\varepsilon)\sin^4\theta) \tag{2-4}$$

Equation (2-4) has three advantages over other traveltime equations: (1) Fast traveltime calculation using the group velocity; (2) Easy generation of Frechet's kernels for inversion; (3) Providing physical insight into the wave propagation in anisotropic media.

Because the anisotropic ray tracing method needs direct measurement of ray angle for traveltime calculation and Equation (2-4) provides the apparent ray angle measured from two neighboring ray tracing nodes with particular symmetry axis, I extended Equation (2-4) to TTI media to calculate traveltime by introducing tilted angle of symmetry axis from Equation (2-4):

$$V_g^{-2}(\theta-\varphi) = V_g^{-2}(0)(1 - 2\delta\sin^2(\theta-\varphi) + 2(\delta-\varepsilon)\sin^4(\theta-\varphi)) \tag{2-5}$$

Where φ is tilted angle of symmetry axis, $(\theta-\varphi) = \gamma$ is the group angle (Figure 2-2).
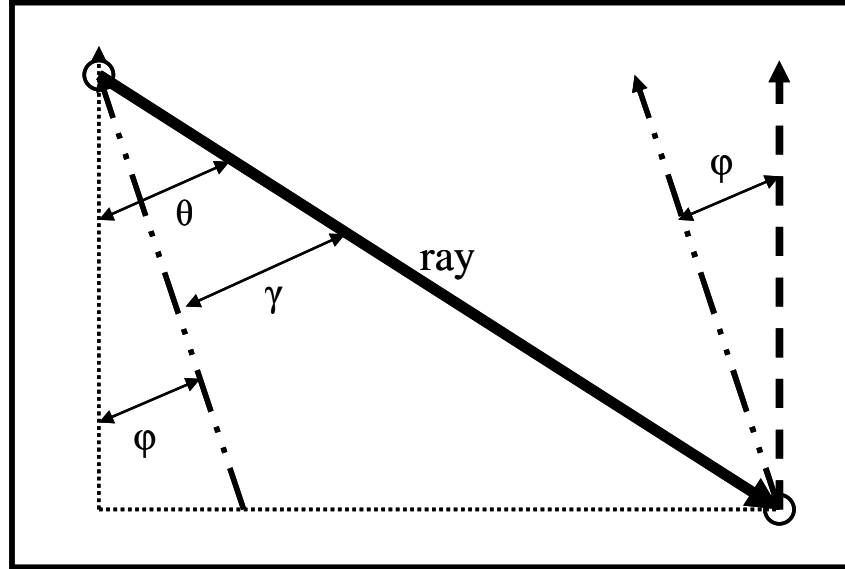
Figure 2-2: A sketch to illustrate TTI model. Variable φ is the tilted angle between vertical axis (dash line) and tilted symmetry axis (long dash dot line), θ is the angle between vertical axis and ray path (solid line), γ is the ray angle, or group angle (θ-φ).

In ray tracing algorithm, the calculated velocity needed to combine with the length of ray path to obtain the traveltime (Appendix A):

$$t = len_{ray} * sw_{p0} * \sqrt{1 - 2\delta \sin^2(\theta - \varphi) + 2(\delta - \varepsilon)\sin^4(\theta - \varphi)} \qquad (2\text{-}6)$$

where t is traveltime and len_{ray} is the distance along the raypath, sw_{p0} is the P-wave slowness along the symmetry axis, or the axial slowness.

2.2.2 Numerical experiments of anisotropic ray tracing

Shortest path ray tracing is based on Huygens' Principle (Musgrave 1970). It describes the basics of wave propagation which is that every point on a wavefront is a new source of secondary waves. For the next wavefront the wave solution is the summation

16

of the contributions from all the 'point sources' on the previous wavefront. Shortest path ray tracing is defined in terms of a directed grapy consisting of *n* nodes, which are numbered *0, …, n-1*. Node *0* is called the "source" (Figure 2-3). From source point to connect different forward points then record the traveltime between those two nodes.
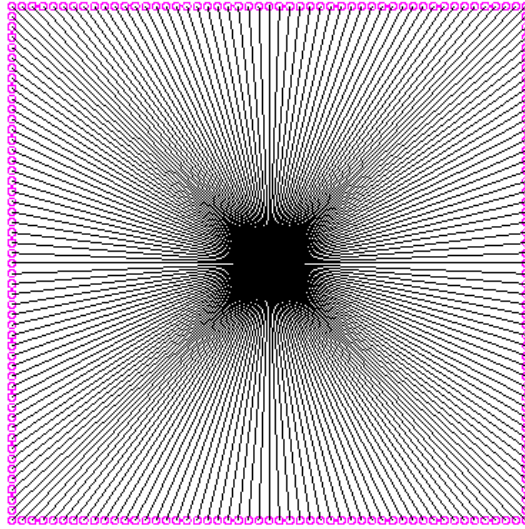
Figure 2-3: The distribution of ray tracing nodes. The source point is located at center of model. Purple points on each side are ray tracing nodes.

In anisotropic media, the nodes distribution can be treated as same with isotropic media. However, because the velocity varies on different directions, the minimum traveltime from source to target point will change. Therefore the forward point can be referred to the one given shortest traveling path. To calculate P-wave traveltime in anisotropic media, Equation (2-6) is combined with the shortest path ray tracing algorithm. Figure (2-4) shows the wavefronts in TTI media with different tilted angle of symmetry axis.
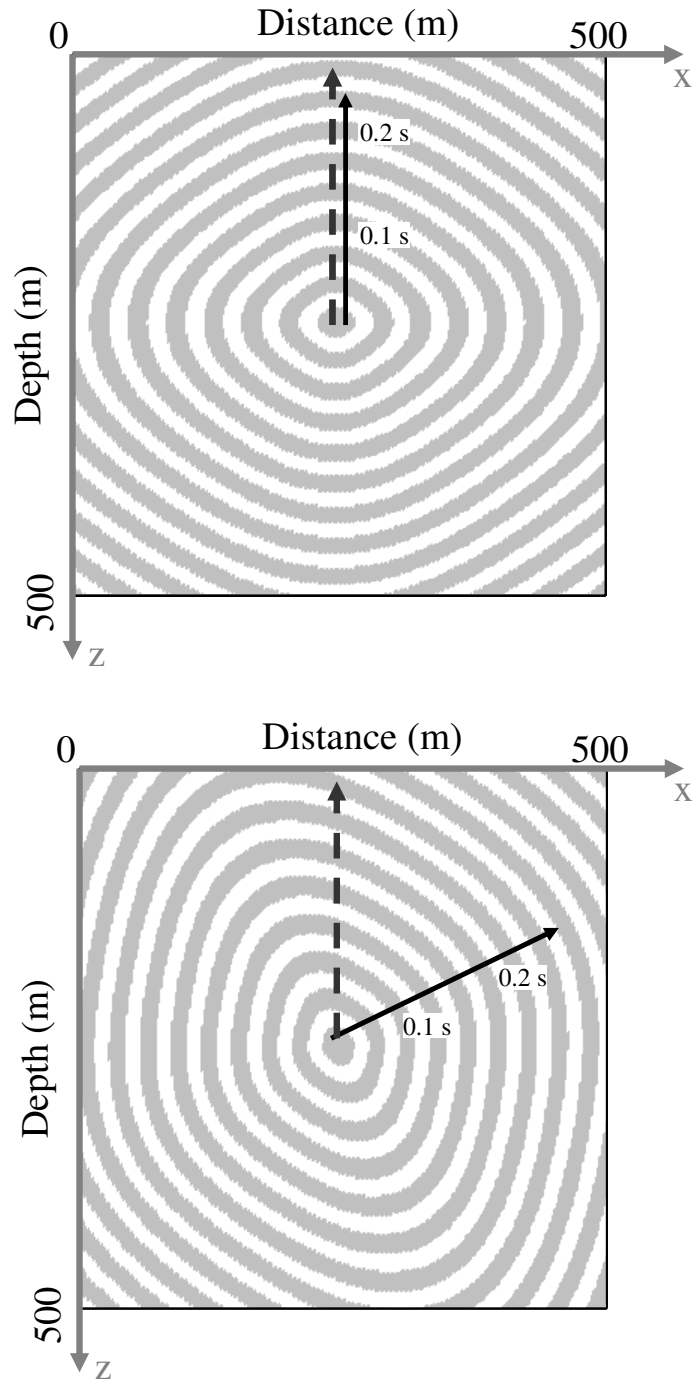
Figure 2-4: The P-wave wavefronts in TI media with the different tilted angle φ, generating by TTI ray tracing. (a) $\varphi = 0°$ (VTI). (b) $\varphi = -67°$. Here $sw_{p0} = 1s/km$, $\varepsilon = 0.18$, $\delta = -0.12$. Dash line presents the vertical axis and solid line represents the direction of tilted symmetry axis.

18

2.2.2.1 Anisotropic ray tracing in 2D TTI media

In multilayered homogeneous anisotropic media, each layer consists of constant anisotropic parameter ε and δ, tilted angle φ of symmetry axis, and axial velocity along symmetry axis. A ray path is a sequence of nodes and connections succeeding each other. The traveltime along a path from one node to another is defined as the sum of the weights of the connections of the path. The final path is the path with smallest possible traveltime. Figure (2-5) shows a comparison of isotropic ray tracing and anisotropic ray tracing in a numerical model from West Africa. In Figure (2-5b), ray paths will derivate from vertical axis depending on how the tilted symmetry axis is assumed. Here, the tilted symmetry axes are approximated to perpendicular to layer bedding in area where steeply dipping exists.
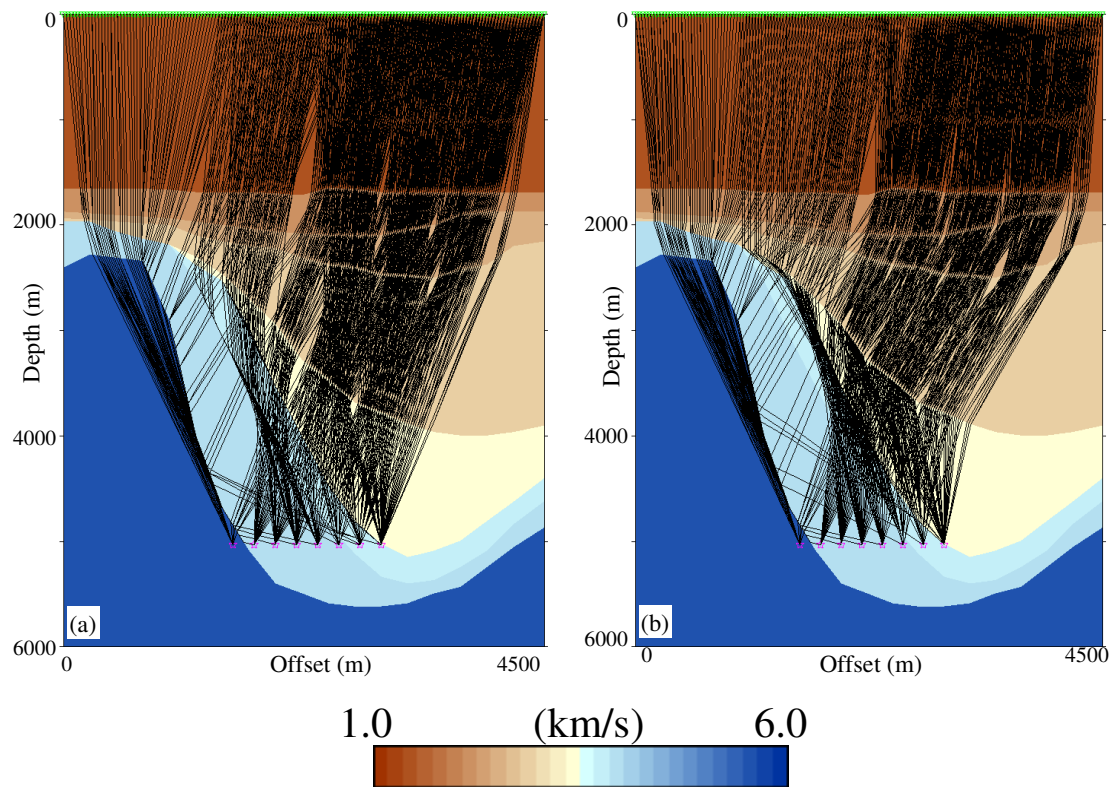
Figure 2-5: Ray tracing in a numerical model from West Africa. (a) Isotropic ray tracing. (b) TTI ray tracing.

2.2.2.2 Anisotropic ray tracing in 3D TTI media

To extend the approach to 3D model, there are two different assumptions on the tilted angle of the anisotropic symmetry axis (Figure 2-6). The first one assumes that each model layer has a constant orientation of the symmetry axis, which is described by the tilted angle φ and azimuth angle Φ. However, geological interpretations indicate that it is rare that the symmetry axis in 3D deformable plane is expressed by only two angles. Some researches took the second assumption that tilted symmetry axis is perpendicular to the orientation of each layer (*e.g.*: Zhou et al. 2004; Zhou, 2006).
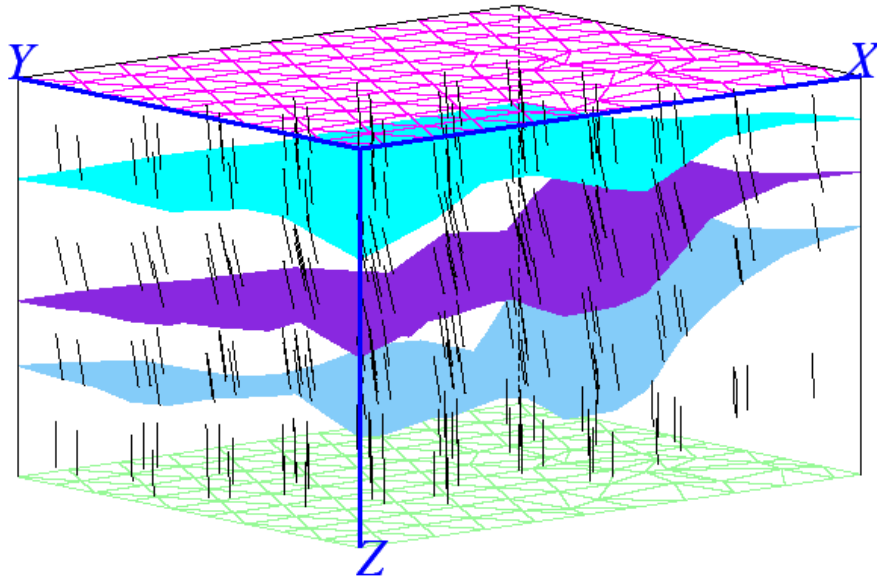
(a)
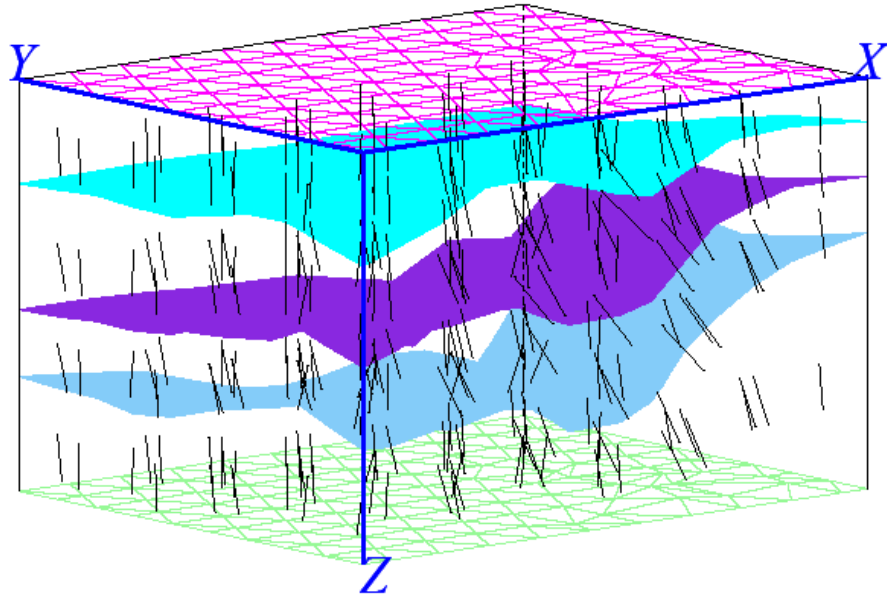
(b)

Figure 2-6: Two assumptions of tilted symmetry axis in 3D layered model. (a) Each layer has constant tilted angle φ and azimuth angle Ψ of symmetry axis. (b) The symmetry axis is always perpendicular to layer interface at each location.

Various approaches have been proposed to divide the interface geometry into triangles, such as Delaunay triangularization (Bohm et al., 2000) and the atomic meshing method (Ruger and Hale, 2006). For traveltime tomography, the proper triangularization can minimize size differences and extreme height base ratios of the triangles and align the edges of the interface triangles with the geological boundaries. Zhou (2006) proposed an adaptive triangularization algorithm for 3D traveltime tomography. If the depth variations of the geological boundaries are known and are significant to the analysis, this adaptive triangularization can allow variable triangular divisions for different model interfaces. Figure (2-7) represents that the model consists of a number of layers based on adaptive triangulation algorithm.
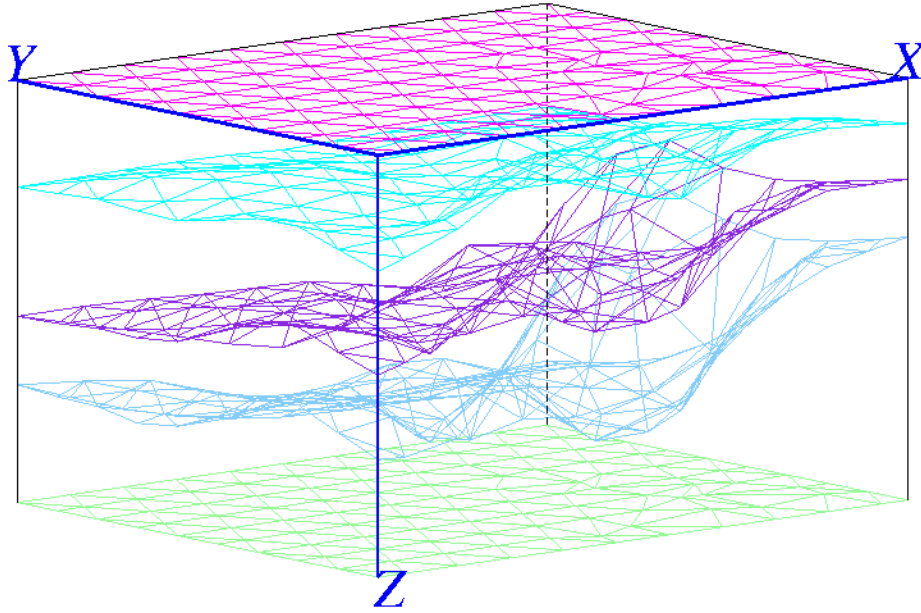
Figure 2-7: 3D layered model with adaptive triangularization algorithm.

In 3D media, with the same assumption of traveltime equation, anisotropic ray tracing in TTI media can be proposed. Figure (2-8) shows the synthetic ray tracing in isotropic and TTI media where tilted symmetry axes are perpendicular to layer geometry in each location.
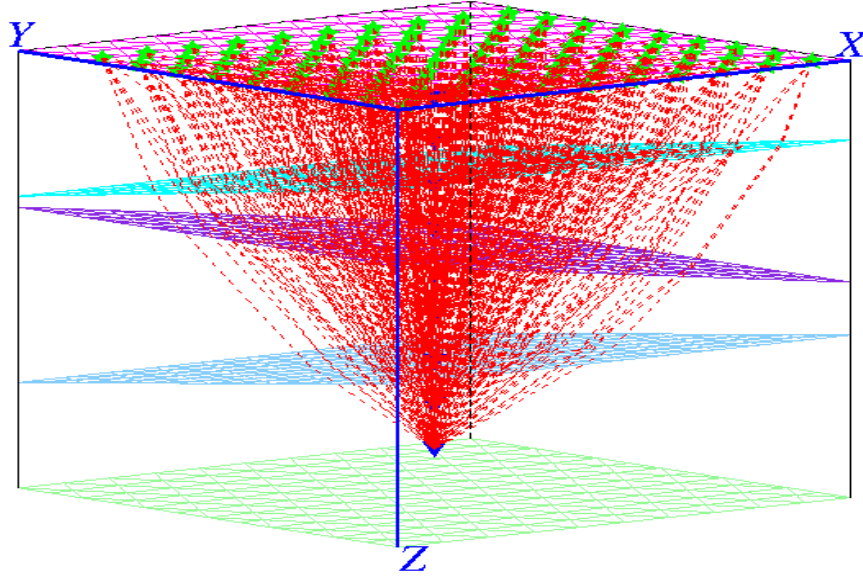
(a) Isotropic ray tracing
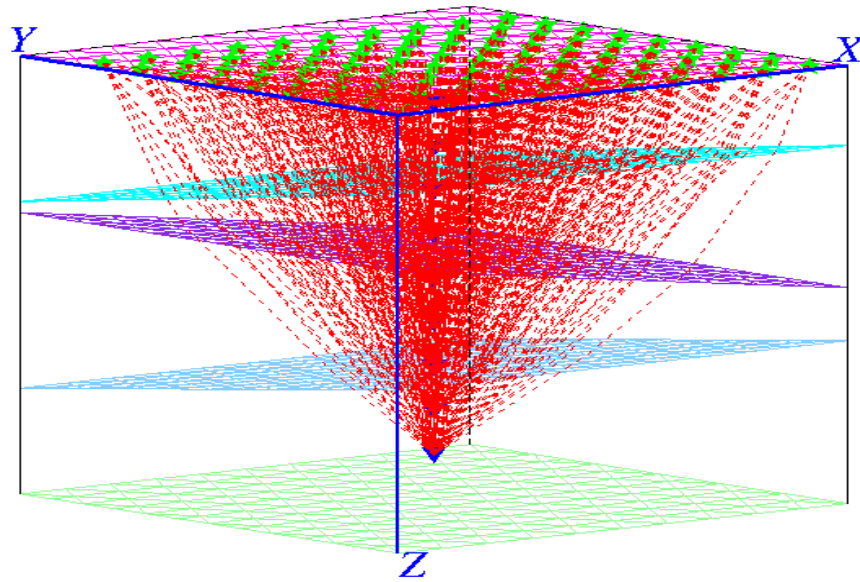
(b) Anisotropic ray tracing

Figure 2-8: 3D ray tracing in isotropic and TTI media. (a) Raypaths (dashed lines) in isotropic model with one vertical well located at the center of model. (b) Raypaths in TTI model with assumption of tilted symmetry axis perpendicular to layer interface. Here, the velocity is {2.0; 3.0; 4.0; 5.0} km/s from top to bottom layer. In (b), ε = {0.18; 0.16; 0.14; 0.12} and δ = {0.15; 0.13; 0.11; 0.09} from top to bottom layer respectively.

2.2.3 Waveform modeling in anisotropic media

Zhou et al (2006a) proposed a new anisotropic acoustic equation which is based on dispersion relation as Alkhalifah's (2000). By introducing an auxiliary function, the fourth order differential equation becomes a coupled second order differential equations:

$$\frac{\partial^2 p}{\partial t^2} = V_p^2 \left\{ (1+2\delta)(\frac{\partial^2}{\partial x^2} + \frac{\partial^2}{\partial y^2})(p+q) + \frac{\partial^2}{\partial z^2} p \right\}$$
$$\frac{\partial^2 q}{\partial t^2} = 2V_p^2(\varepsilon - \delta)(\frac{\partial^2}{\partial x^2} + \frac{\partial^2}{\partial y^2})(p+q)$$

(2-7)

Here p is P wavefield and q is an auxiliary wavefield to compensate the loss of anisotropy for VTI media.

By eliminating the propagation items along y direction, Figure (2-9) shows the different snapshots generated by Equation (2-7) in 2D VTI media.
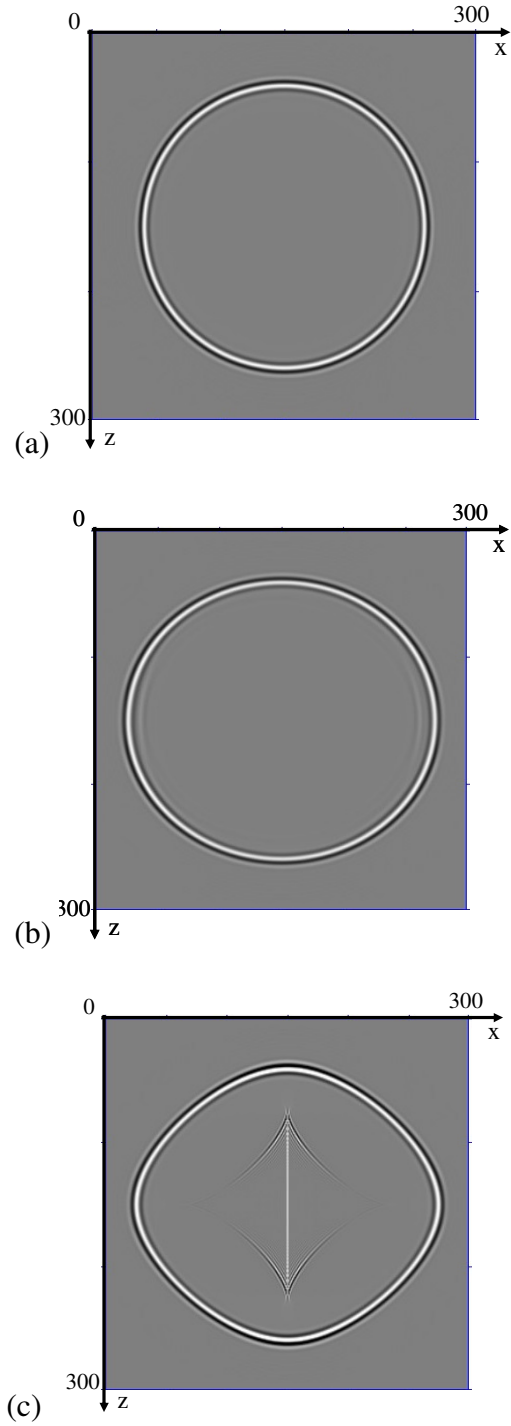
Figure 2-9: (a) ε = 0.0, δ=0.0; (b) ε = δ= 0.15; (c) ε = 0.15, δ=-0.15. The source wavelet is Ricker wavelet with maximum frequency 60Hz. All three snapshots are recorded at t=0.3 s and Vp_0=1.0 km/s.

One can notice that there is a diamond-shaped wave appearing in the middle of the VTI wave field. It is caused by the solution of VTI wave equation. This additional wave, which only appears in anisotropic media, has been discussed in many papers (Alkhalifah, 2000; Grechka et al., 2004). Alkhalifah (2000) experimented that when the source point is located at isotropic media above the VTI media, the artifact will disappear (Figure 2-10).
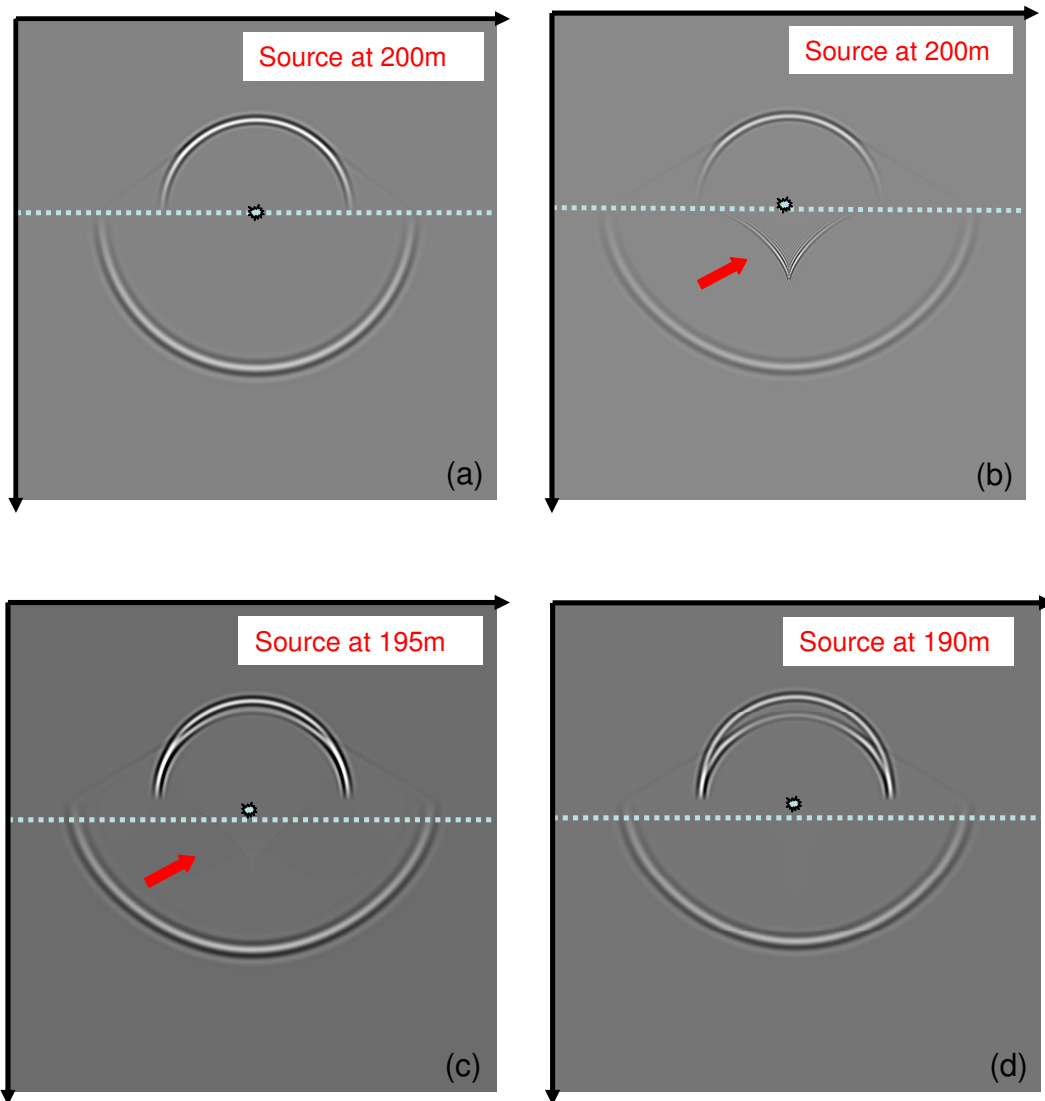
Figure 2-10: The wave field at 0.8 s is caused by a source at a central lateral location. The model consists of two layers. The first layer is isotropic with v =1.5 km/s, the second layer (in b, c and d) is VTI with v =2.5 km/s, ε=0.2 and δ=0.05. The reflector is at 200 units. The source depth varies with (a) the source is at 200 units in isotropic model, (b) the source is at 200 units in VTI model, (c) the source is at 195 units VTI model, and (d) the source is at 190 units in VTI model. The additional wave decays gradually with increasing distance between the source and the VTI layer.

Figure (2-11) shows the snapshots of waveform modeling in a synthetic 3D VTI media. In VTI media, seismic waves will propagate faster along horizontal direction. Because ε controls the difference between horizontal and vertical velocity, strongest ε will provide fastest wave velocity at horizontal direction. This may impact picking of first arrivals and result in errors for parameter estimation.

(a)

(b)

(c)   (d)
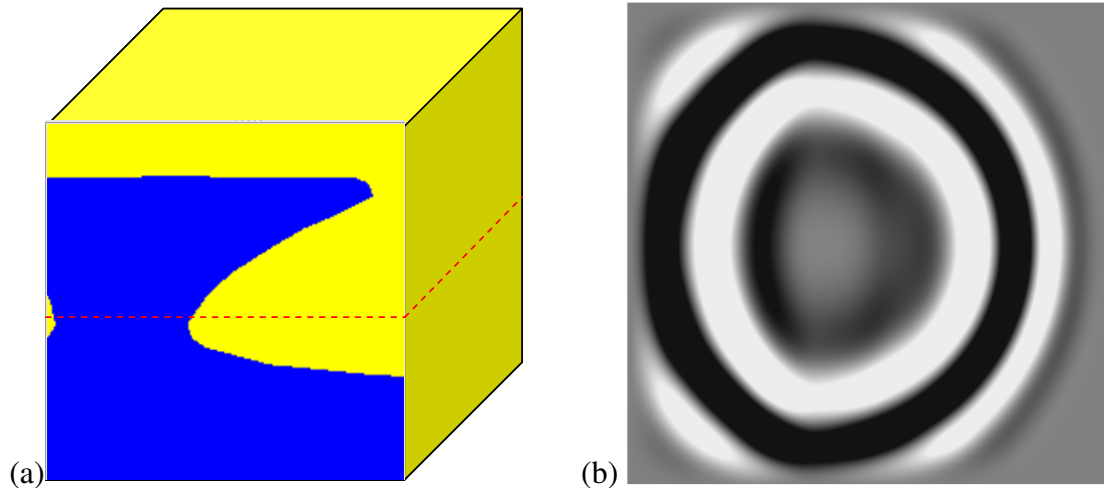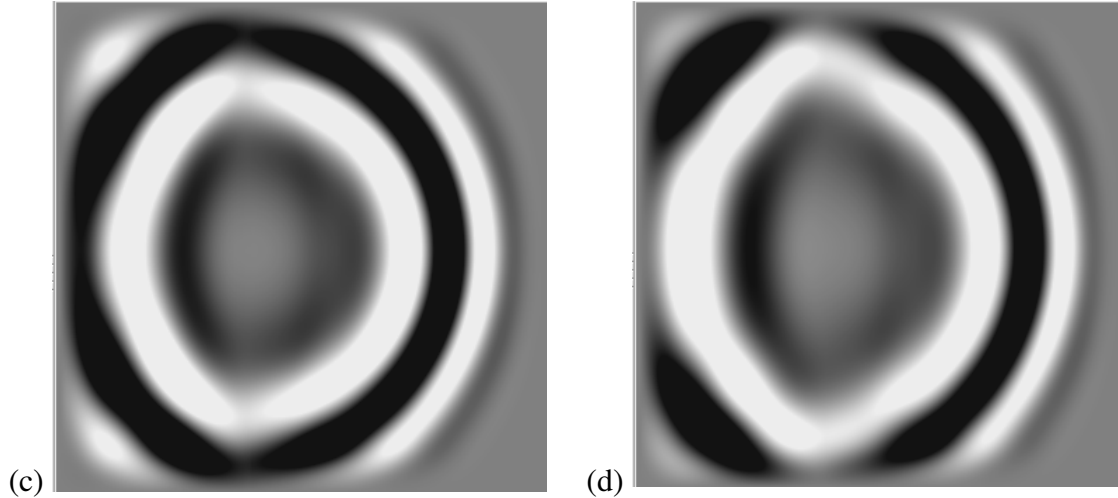
Figure 2-11: Depth slices of waveform in 3D VTI media. (a) 3D velocity model assuming blue area is anisotropic. (b) Depth slice when $\varepsilon = \delta = 0.0$; (c) depth slice when $\varepsilon = 0.1$ and $\delta = 0.05$; (d) depth slice when $\varepsilon = 0.2$ and $\delta = 0.2$. The red dashed box in (a) is the depth of each slice. Assuming blue area is VTI media.

Although VTI media is a good approximation of anisotropic model, it is only for simple geological model. When sedimentation and tectonic processes produce dip and thickness variations in rock layers, their velocity structures may be approximated as TTI media. Since Alkhalifah (2000) introduced the "acoustic" approximation for VTI media, it has attracted many geophysicists to continue to work on it for modeling and migration in TTI media (Zhou et al., 2006b; Zhang et al., 2006; Du et al., 2007). After taking into account the tilted angle in TI media, Zhou et al. (2006b) proposed an acoustic wave equation in TTI media:

$$\frac{1}{v_0^2}\frac{\partial^2 p}{\partial t^2} - (1+2\delta)Hp - H_0 p = (1+2\delta)Hq$$

$$\frac{1}{v_0^2}\frac{\partial^2 q}{\partial t^2} - 2(\varepsilon - \delta)Hq = 2(\varepsilon - \delta)Hp$$

where $\hspace{8cm}$ (2-8)

$$H = \cos^2\varphi\frac{\partial^2}{\partial x^2} + \sin^2\varphi\frac{\partial^2}{\partial z^2} - \sin 2\varphi\frac{\partial^2}{\partial x\partial z}$$

$$H_0 = \sin^2\varphi\frac{\partial^2}{\partial x^2} + \cos^2\varphi\frac{\partial^2}{\partial z^2} + \sin 2\varphi\frac{\partial^2}{\partial x\partial z}$$

Figure (2-12) shows a TTI waveform modeling generated by Equation (2-8) when tilted angle of symmetry axis is 30°.
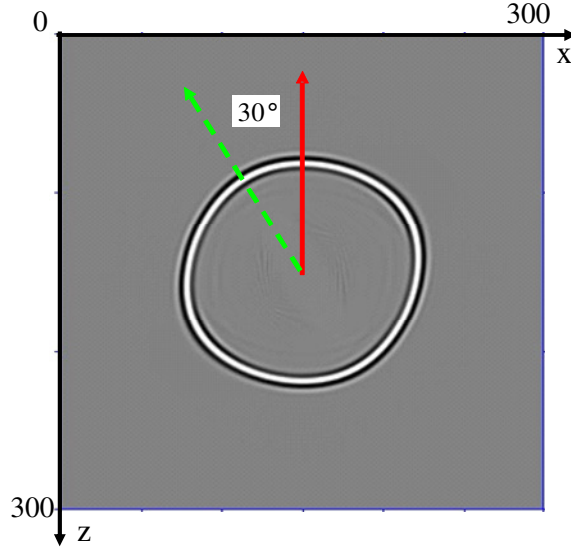
Figure 2-12: Snapshot of 2D TTI waveform modeling. Here, $\varepsilon = 0.1$, $\delta = -0.1$, $\varphi = 30°$.

To facilitate traveltime inversion, Figure (2-13) shows a comparison between the ray tracing and waveform modeling results in a multi-layer TTI model. The first arrivals from the ray tracing are in good agreement with the first arrivals generated using Equation (2-8) for the same anisotropic model. The small difference at near surface is due to the source delay and limited frequency in waveform modeling. Anisotropic ray

tracing estimates accurate traveltime with less computation time than waveform modeling in this case. Overall, the comparison demonstrates that the TTI ray tracing provides accurate result and takes less computation time and memory than the waveform modeling.

(a)

	Vp_0(km/s)	ε	δ	φ
Layer1	2.0	0.10	-0.04	20°
Layer2	2.5	0.12	-0.06	30°
Layer3	3.0	0.14	-0.08	40°
Layer4	3.5	0.16	-0.10	50°

(b)
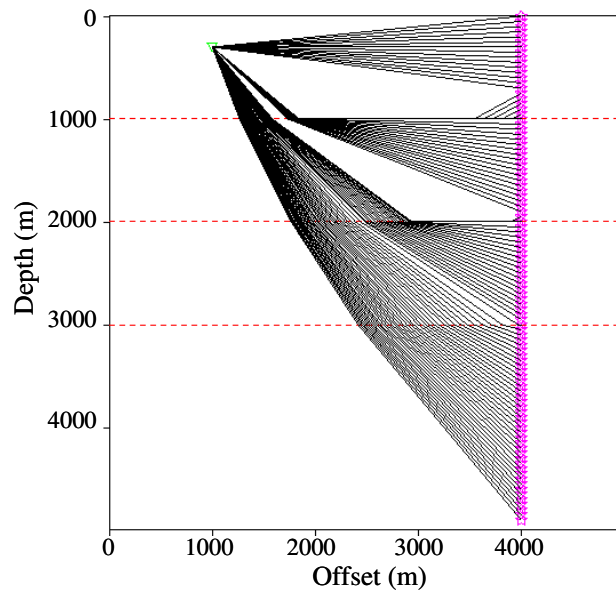
(c)
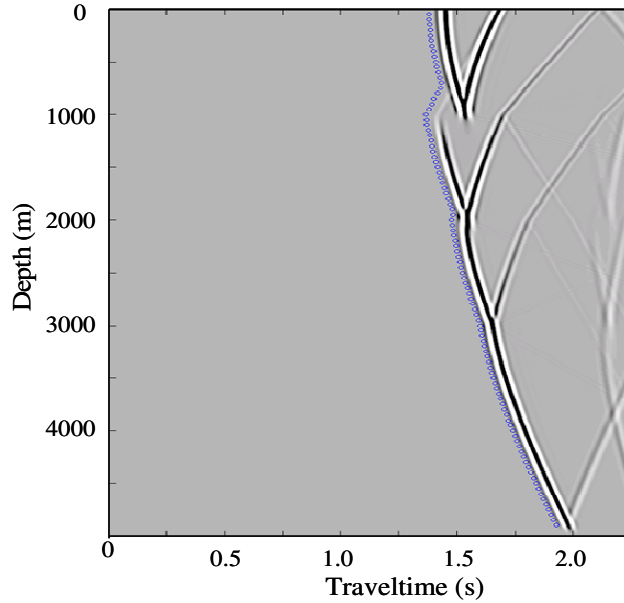
Figure 2-13. The comparisons between TTI ray tracing and TTI waveform modeling. (a) Anisotropic parameters in each layer. (b) TTI Ray tracing. (c) Common shot gather generated by TTI finite difference waveform modeling. The dotted line indicates the picked first arrival traveltime from (b).

2.3 CHALLENGES OF ANISOTROPIC FORWARD MODELING

2.3.1 Challenges of anisotropic ray tracing

The computation time of anisotropic ray tracing is mainly depends on the density of ray tracing nodes placed on the boundaries. The sparser ray tracing nodes have, the faster computation time will be. However, the trade off between computational time and accuracy become an issue in terms of traveltime calculation. The proper setting of ray tracing nodes will provide acceptable computation time and accurate results. In 3D model, the ray tracing nodes only need to be placed on the facets of the triangular prisms. If velocity gradient is introduced for each layer (Liu et al., 2009a, 2009b), more ray-tracing nodes must be placed inside each layer which will increase great computational time. In shortest path ray tracing algorithm, the number of ray tracing

31

nodes is adjustable when applying in the tomographic inversions. It provides the optimized solution from trade offs of computational time and accuracy.

One of the limitations of this anisotropic ray tracing approach is that it can not generate triplication effects when dealing with S-wave ray tracing. The reason is because shortest path ray tracing algorithm only considers first arrivals. This limitation can be avoid by applying shooting method or replaced with waveform modeling to obtain traveltime data when S-wave information is necessary.

2.3.2 Challenges of anisotropic waveform modeling

Due to the pseudo-acoustic approximation on the elastic wavefield for VTI and TTI media, the diamond-shape artifacts is clearly present (Figure 2-9c). Such artifacts can be suppressed by placing the source in isotropic layers . However, the strong variations of dip angle and azimuth in terms of the tilted axis of symmetry can cause wave propagation to be unstable (Zhang and Zhang, 2009). Flectcher et al. (2009) proposed an alternative method which is adding a finite shear wave velocity to help wave propagation not blow out, but the shear wave exists in P-wave propagation (Jin et al., 2010). However, Flectcher et al.'s approximation (2009) will increase computation time and memory requirement. With rapid development of computer hardware, it is still promising and increasingly feasible to apply anisotropic waveform modeling and migration in industry production application.

2.4 CHAPTER SUMMARY

In this chapter, the algorithms of 2D/3D shortest path ray tracing algorithms in TTI media are developed. A direct extension from Sena's equation (1991) into TTI media

can generate accurate first arrivals compared with finite difference waveform modeling. The new TTI traveltime equation has advantages on fast traveltime calculation using the group velocity, and it is capable to easily generate of Frechet's kernels for tomographic inversion.

In 2D TTI media, the anisotropic ray tracing is capable to handle the arbitrarily tilted axis of symmetry. To best describe the subsurface structure, the assumption of tilted symmetry axis perpendicular to layer bedding is more proper for ray tracing approach in 3D media. The numerical results illustrate that the anisotropy significantly affects the ray trajectory in the media, considering anisotropy in particular allows us to understand the location of the transmission or reflection points for different tilted axes of symmetry.

CHAPTER 3: ANISOTRPIC TRAVELTIME TOMOGRAPHY IN VTI/TTI MEDIA

3.1 INTRODUCTION

Seismic tomography, a methodology of estimating the Earth's properties, has been applied to solid Earth sciences and exploration seismology. There are two main types of seismic data to be inverted by tomography: traveltime data and waveform data. Traveltime data is used to reconstruct Earth's velocity models with lower resolution compared with waveform data. However, traveltime tomography is robust and easy to implement with fast computation ability.

In solid Earth sciences, traveltime tomography is extended to reach the inversion of the Earth's eigenfrequencies and dispersion properties of long-period surface waves, using perturbation theory on normal modes. By 1984, Woodhouse and Dziewonski (1984) began to use long-period data to image the upper mantle using the lowest order spherical harmonics. This led to an immensely fruitful era in which the large scale structure of the Earth was mapped in increasing details.

In exploration seismology, ray-based tomography has become the standard model building tool for seismic depth imaging. With the increasing of computer power, the evolution of tomography has been driven by exploration demands (*e.g.*: Li et al., 2008; Woodward et al., 2008, Zhou et al., 2008). Standard model resolution has increased from a few thousand meters to a few hundred meters. This allows us to obtain high

quality, complex residual moveout data as densely as 50m horizontally and vertically. The multiple azimuth dataset can help to improve illumination and multiple suppressions (Zou et al., 2008) by high resolution traveltime tomography. In recent years, a shift from conventional isotropic to predominantly anisotropic model becomes necessary to provide accurate subsurface model, such as subsalt and thrust fault, for depth migration.

Layered tomography was developed primarily for reflection imaging (Bishop et al., 1985; Kosloff et al., 1996). It can be used to update the geometry of velocity interfaces using the residual traveltimes of reflector. Layered tomography is applicable where geological features such as weathering zones, stratigraphic units, and salt bodies can be represented easily by layers (Zhou, 2006). It has potential to constrain the geometry of velocity interfaces in areas with nearly parallel rays.

In this chapter, first arrival traveltime tomography algorithm in 2D/3D TTI media is developed. The derived analytical kernels represent the sensitivities of each anisotropic parameter in terms of traveltime. Such kernels directly indicate the observation of the structural parameters by analyzing their spatial distribution patterns. Several synthetic experiments show some combinations of anisotropic parameters can be invert successfully. The inversion results are necessary for depth migration.

3.2 ANALYSIS OF FRECHET KERNELS ON TRAVELTIME DATA

To investigate the earth's structure, finite-frequency Frechet kernels for surface wave phase velocities and body wave traveltime from earthquakes have been discussed (Marquering et al., 2002; Zhou and Greeenhalgn, 2009). Such kernels directly indicate the sensitivity of the observations to the inversion parameters by analyzing the spatial

distribution patterns. Frechet kernels are also sensitive when different acquisition geometries involved which is referred to the variation of incident angles. The calculated Frechet derivatives can be used for a model parameterization explicitly and directly used in any local search minimization inversion algorithm, such as conjugate gradient or Gauss-Newton to yield the elements of the Jacobian matrix directly for arbitrary model parameterization.

3.2.1 Derivation of Frechet TTI kernels on traveltime data

The TTI parameters consist of the anisotropic parameters ε and δ, the tilted angle φ of their symmetry axis, layer velocity or slowness along the symmetry axes, and the thickness variation of the layer. To derive a set of TTI kernels for anisotropic tomography, recall the Equation (2-5):

$$t = len_{ray} * sw_{p0} * \sqrt{1-2\delta\sin^2(\theta-\varphi)+2(\delta-\varepsilon)\sin^4(\theta-\varphi)}$$

The TTI kernels can be derived by the first derivative of Equation (2-5) over relative TTI anisotropic parameter (Appendix B):

The kernel for slowness is derived as:

$$\frac{\partial t}{\partial(sw_{p0})} = len_{ray} * (1-2\delta\sin^2\gamma+2(\delta-\varepsilon)\sin\gamma^4)^{\frac{1}{2}} \tag{3-1}$$

The kernels for anisotropic parameters ε and δ are derived as:

$$\frac{\partial t}{\partial \varepsilon} = \frac{-(len_{\mathrm{ray}} * sw_{\mathrm{p0}} * \sin^4 \gamma)}{\sqrt{1 - 2\delta\sin^2\gamma + 2(\delta - \varepsilon)\sin^4\gamma}} \tag{3-2}$$

$$\frac{\partial t}{\partial \delta} = \frac{len_{\mathrm{ray}} * sw_{\mathrm{p0}} * (\sin^4 \gamma - \sin^2 \gamma)}{\sqrt{1 - 2\delta\sin^2\gamma + 2(\delta - \varepsilon)\sin^4\gamma}} \tag{3-3}$$

In deriving the kernel for the tilted angle of the symmetry axis, taking the sine function of the tilted angle φ as the variable to obtain

$$\frac{\partial t}{\partial(\sin\varphi)} = len_{\mathrm{ray}} * sw_{\mathrm{p0}} *$$

$$\frac{\left[2\delta\sin\gamma(\sin\theta\,\mathrm{tg}\varphi + \cos\theta\cos\varphi) + 4(\varepsilon - \delta)\sin^3\gamma(\sin\theta\,\mathrm{tg}\varphi + \cos\theta\cos\varphi) \right]}{\sqrt{1 - 2\delta\sin^2\gamma + 2(\delta - \varepsilon)\sin^4\gamma}} \tag{3-4}$$

Finally for the interface k_z_{il}, the analytical formulation is not available, except for simple cases (*e.g.*, Kosloff et al., 1996; Zhou, 2003). Here, the interface kernels are estimated numerically following Zhou (2006). The calculated Frechet derivatives can be used for a model parameterization explicitly and directly used in any local search minimization inversion algorithm, such as conjugate gradient (Scales, 1987) or Gauss-Newton (Pratt et al., 1998) to yield the elements of the Jacobian matrix directly for arbitrary model parameterization. Each Frechet kernel presents the rates of change in the observations to perturbations in cell or medium properties, such as Thomsen's anisotropic parameter. Therefore, the Frechet kernels are examined as sensitivity

functions of the data to a particular parameter and indicate the sensitivity variations with various surveying configurations (Zhou and Greenhalgh, 2009).

3.2.2 The sensitivity of Frechet TTI kernels on variation of ray angles

Each of the above kernels depicts the sensitivity of the traveltime to the corresponding inversion variable, hence quantifying the resolvability for the variable. Based on the analytical kernels, the sensitivity of traveltime to key TTI parameters as a function of the ray angles for a specified set of anisotropic parameters is shown in Fig. 4. At the same ray angle, the sensitivity of the traveltime to different TTI parameters can be quite different. For instance, the axial velocity has best sensitivity in all ran angle range, it can be considered as first priority inversion parameter in any acquisition geometry. The kernel for ε reaches to a high peak around ray angle 90°, meaning that ε is most resolvable using rays along the direction normal to the tilt symmetry axis, meaning that crosswell geometry may be the best acquisition geometry to resolve ε. The kernel for δ reaches to its peak around ray angle 45°, hence it indicates that δ is most resolvable using rays along 45° direction, or in VSP acquisition geometry. The kernel for sine function of tilted angle φ reaches to a broad peak with intermediate magnitude between ray angle 60° and 80°, indicating it has a similar sensitivity trend but less tolerant to noise in comparison with that for ε. Since the magnitude of the kernel for ε is much greater (more than four times in this case) than that for δ in the range of large ray angles, it is generally much easier to use traveltimes to invert for ε than for δ in crosswell geometry, but the reversed assumption in VSP acquisition geometry. The tilted angle φ shows the average resolvability in both VSP and crosswell geometries, it could be inverted after estimating ε in crosswell geometry or estimating δ in VSP geometry. Though a simple anisotropic model with one set of the parameter values is used to show the sensitivity of the traveltime to the inversion

variables here, we may expect similar trend in the sensitivity for more complicated TTI models as mosaics of the simple model.
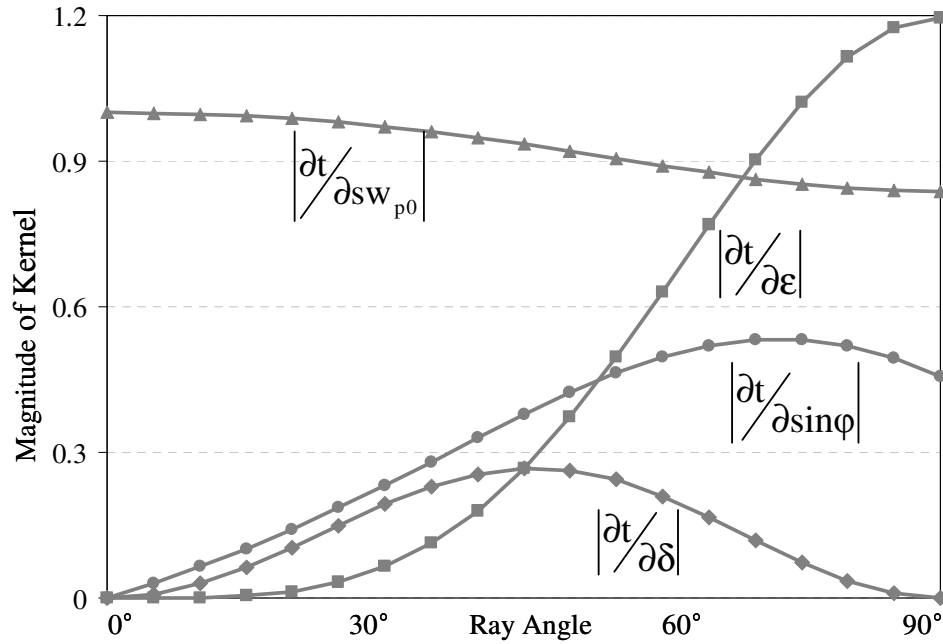
Figure 3-1: The sensitivity of traveltime to key TTI parameters as a function of the ray angles. Here, $sw_{p0} = 1$ s/m, $len_{ray} = 1$ m, $\varepsilon = 0.15$ and $\delta = 0.1$ for calculating kernels using Equation (3-1) – (3-4). The kernel of sine function of tilted angle φ is calculated with assumption of 45° tilted angle.
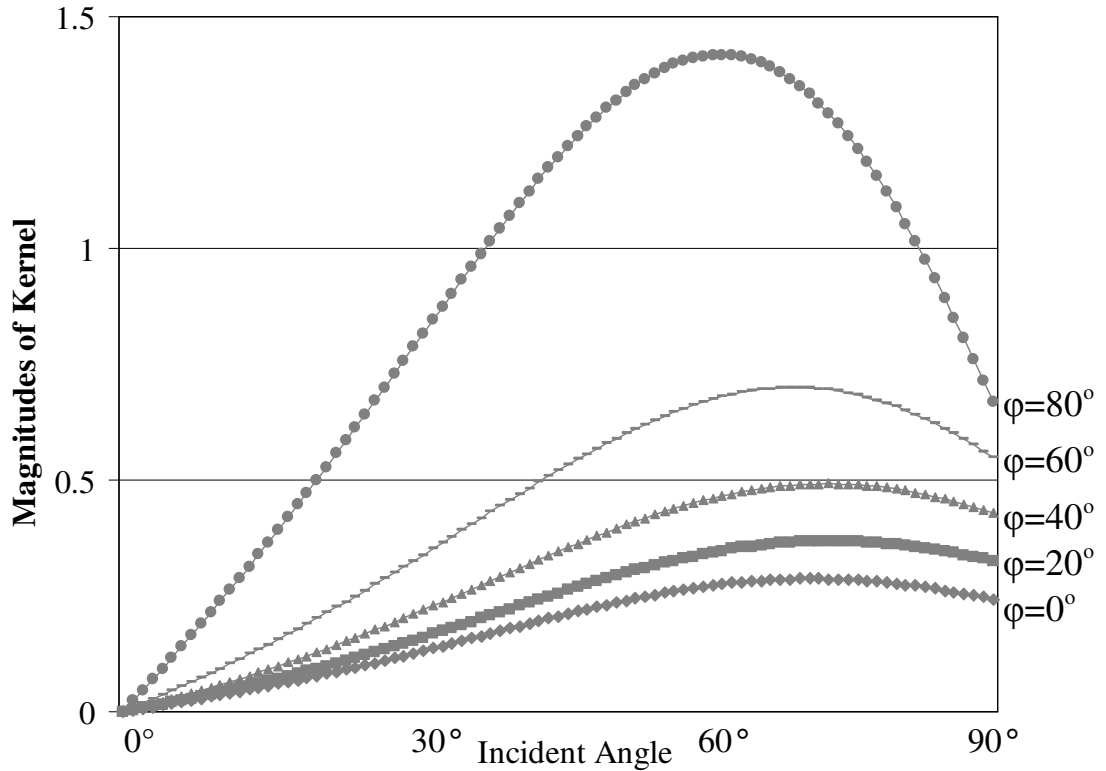
Figure 3-2: Different kernels of sine function of tilted angle φ when ray angle changes.

To calculate the numerical kernels of layer geometry, the ray nodes on the interface will be moved by a small vertical perturbation of Δz. The refraction kernel is estimated as the ratio of the traveltime difference between refraction raypath SRT and SR'T over the vertical perturbation Δz (Figure 3-3) . Figure (3-4) illustrates the sensitivity of numerical kernel on the different incident angles. Although it only shows part of incident angle, the general trend indicates that the kernel of layer geometry is sensitive with traveltime when incident angle become larger. Therefore, crosswell or VSP acquisition geometry should be considered as preferred recording geometry for estimating layer geometry.
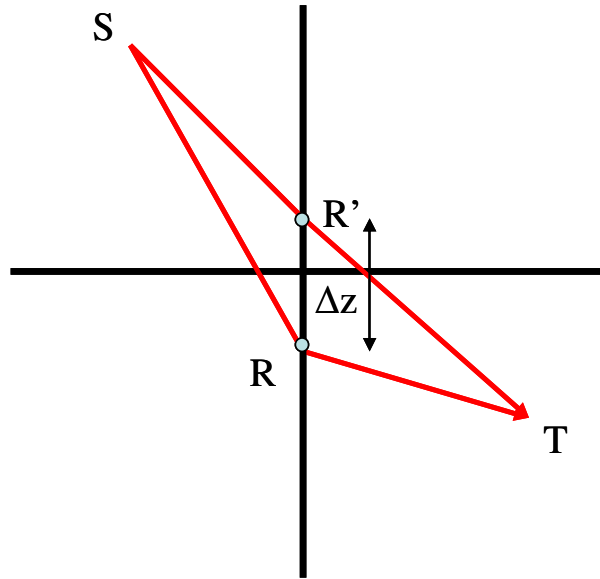
Figure 3-3: Numerical calculation of the layer geometry kernels for a node R. Node R is moved to R' by a small perturbation Δz. The refraction kernels are estimated as the ratio of the traveltime difference between refraction raypath SRT and SR'T over the vertical perturbation Δz.
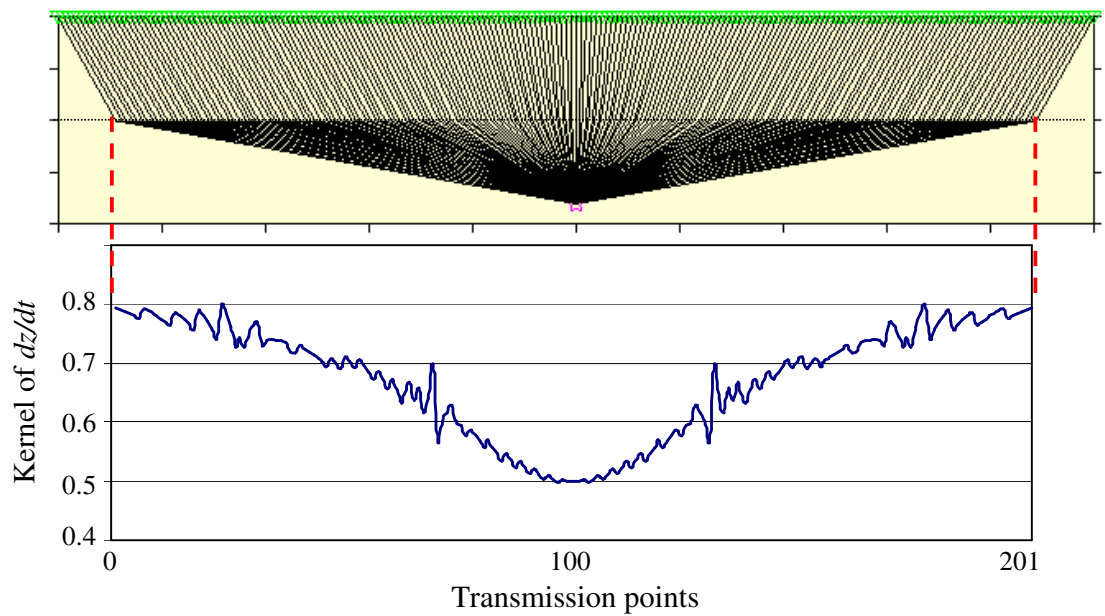
Figure 3-4: The numerical kernel of layer geometry. (Upper) Transmitted rays in 2-layer velocity model. (Lower) The corresponding numerical kernels.

3.3 LAYERED TRAVELTIME TOMOGRAPHY IN VTI/TTI MEDIA

Anisotropic traveltime tomography uses traveltimes of seismic waves to constrain anisotropic velocity variations. Cell-based anisotropic tomography inverts for velocity and anisotropic parameters as a function of spatial location. The velocity is resolvable where there are a sufficient number of intersecting rays. However, poor ray angle coverage leads to smear artifacts bearing the imprint of the raypaths and poor resolution of anisotropic anomalies (Cerveny, 2001). Therefore, layered tomography was developed to update the geometries of velocity interfaces using residual traveltimes of reflectors (Bishop et al., 1985; Kosloff et al., 1996). It avoids the problems of smearing artifacts and it is applicable where geological features can be represented easily by layers, such as weathering zones, stratigraphic units, and salt bodies.

Zhou (2006) proposed a layered tomography named Deformable Layer Tomography, or DLT. A conventional DLT model consists of a number of layers based on a stratigraphic interpretation. This approach can be used to invert for layer velocities and interface geometry simultaneously. The traveltime residual for the ith ray can be represented as:

$$\delta t_i = \sum_j^J k\_s_{ij} \delta s_j + \sum_l^L k\_z_{il} \delta z_l \qquad (3\text{-}5)$$

where δs_j is the slowness perturbation of the jth layer cell, k_s_{ij} is the slowness kernel, δz_l is the interface perturbation at the lth node, and k_z_{il} is the interface kernel. J is the total number of slowness cells and L is the total number of the interface nodes to be

inverted. The introduction of anisotropy brings one more term to the traveltime equation:

$$\delta t_i = \sum_j^J k\_s_{ij} \delta s_j + \sum_l^L k\_z_{il} \delta z_l + \sum_g^G k\_\xi_{ig} \delta \xi_g \tag{3-6}$$

where $\delta \xi_g$ is the perturbation of the gth TTI parameters, such as ε, δ or the titled angle φ, and k_ξ_{ig} is the corresponding kernel. Equation (3-6) describes that in anisotropic layered traveltime tomography the residual traveltime is compound with axial velocity, layer geometry, anisotropic parameters ε, δ and tilted symmetry axis. The variation in one of those parameters will affect the total residual traveltime. Nonuniqueness between those five parameters becomes unavoidable and there is a need to declare the sensitivity of each parameter on the traveltime to estimate the most error-tolerant parameter.

In traveltime tomography, each iteration consists of ray tracing in current reference model to compute the Frechet kernels (anisotropic kernels) and traveltime residuals, inverting for model updates and assessing data-fitting statistics and model variations (Figure 3-5). The calculations of the data fit provide the criteria to terminate the iteration and to select best model as output.

10

The flowchart contains the following boxes:

- Anisotropic ray tracing in TTI media
- Calculated traveltime (lab data)
- Observed traveltime (field data)
- Compare calculated traveltime and observed traveltime, obtain residual traveltime and computer Frechet kernels

$$\delta t_i = \sum_j^J k\_s_{ij}\delta s_j + \sum_l^L k\_z_{il}\delta z_l + \sum_g^G k\_\xi_{ig}\delta\xi_g$$

$$\xi_g \Rightarrow \varepsilon \ or \ \delta$$

- Invert for different anisotropic parameters depending on objectives
- Reach iteration limit? — no / yes
- Output and QC final anisotropic model

Figure 3-5: Flowchart of the anisotropic traveltime tomography.

3.4 NUMERICAL EXAMPLES OF ANISOTROPIC LAYER TOMOGRAPHY IN 2D MEDIA

Following examples show the feasibility of anisotropic layer tomography to estimate interval anisotropic parameters, which include the velocity along the symmetry axis, the thickness-varying interface, Thomsen's two anisotropic parameter ε and δ, and the tilted angle φ of the symmetry axes. Because inverting for all five parameters

simultaneously can bring nonuniqueness and unstable results, each experiment is assigned to invert for different combinations of anisotropic parameters, such as inverting for the velocity along the symmetry axis plus Thomsen's parameters ε and δ together, or inverting for the thickness-varying interface plus the tilted angle φ of the symmetry axis. By adding random Gaussian noise, the inversion results indicate the feasibility of anisotropic layer tomography in field data application.

3.4.1 Crosswell anisotropic tomography in single-cell model with noise-free data

The experiment begins with the simple case of a 2D TTI layered traveltime tomography in a block model. The simulation is to determine anisotropic properties in a single piece of rock that has a set of pre-defined anisotropic parameters. We use crosswell geometry and a combination of crosswell plus VSP acquisition geometry (Figure 3-6) that give different patterns in raypath coverage. The noise-free data, computed by anisotropic shortest path ray tracing, are used as the observed data to examine how accurately the parameters can be recovered by inverting the axial velocity, anisotropic parameters ε and δ, and the tilted angle φ of the symmetry axis together. The values of the model parameters in the initial reference model differ much from that in the true model. Table 3-1 lists the values for one of the inversion tests by TTI layered traveltime tomography. In this case all of the inversion parameters are resolved very well because the good ray coverage.
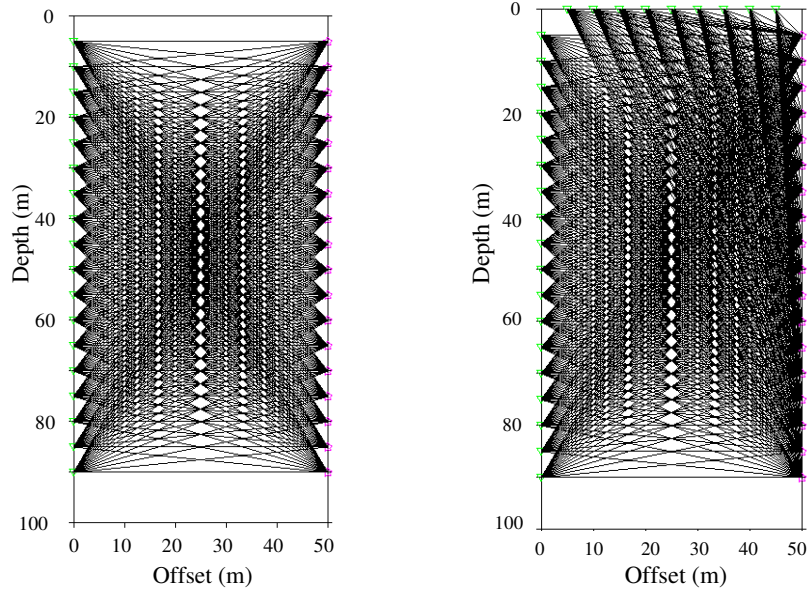
Figure 3-6: Two seismic recording geometries and their relative raypaths in a single block model. (a) Crosswell geometry. (b) Crosswell plus VSP geometry. The triangle indicates the source, and the star indicates the receiver.

Table 3-1: Anisotropic parameters in a 2D single block model and solutions using two different recording geometries.

	True model	Initial model	Crosswell solution	Crosswell plus VSP solution
V_{p0} [km/s]	2.0	2.5	2.003	2.000
ε	0.15	0.0	0.150	0.150
δ	0.10	0.0	0.101	0.100
φ [°]	25	0	24.999	25.000

3.4.2 Crosswell Anisotropic Tomography in Single-cell Model with 5% Gaussian Noise

In this example, the 5% random Gaussian noise is added into input traveltime data in each case (Crosswell only and Crosswell plus VSP). In each case, I invert for the axial

velocity, anisotropic parameters ε and δ together while the tilted angle φ of symmetry axis is fixed. Table (3-2) shows the inversion results from two different acquisition geometries. Although the overall quality of inversion results is decreased, those parameters are still in acceptable range.

Table 3-2: Anisotropic parameters in a 2D single block model and solutions using two different recording geometries with 5% Gauss noise.

	True model	Initial model	Crosswell solution	Crosswell plus VSP solution
V_{p0} [km/s]	2.0	2.5	2.051	2.009
ε	0.15	0.0	0.132	0.145
δ	0.10	0.0	0.030	0.088

In this test, inverted ε is better than δ because large ran angles which is identical with the analysis of Frechet kernel. By adding VSP acquisition geometry on crosswell geometry, the precision of inverted δ has significantly increase. This may indicate that VSP could be a necessary acquisition geometry e acquisition geometry of Crosswell plus VSP provides large ray angle, the inversion results are better than that of only Crosswell. Therefore, to efficiently estimate anisotropic parameters, the acquisition geometry that provides wider ray angle coverage is preferred.

3.4.3 Crosswell anisotropic tomography in multi-layer media with noise-free data

Crosswell tomography provides wide ray angle coverage for detecting anisotropy. I further show a crosswell tomographic inversion for the interface geometry, ε and the tilted angle φ (Figure 3-7). two inversions are experimented with different δ assumptions to test the robustness of the approach. In inversion I (Figure 3-7c), δ is assumed to be correct value in each layer, however in inversion II (Figure 3-7d), δ is assumed to be zero in each layer and is considered as noise in data space.

Both inversions show good approximations. Inversion I is well resolved with the average solution errors of 0.58% for ε and 0.45% for tilted angle φ. The average solution errors for inversion II are 1.8% for ε and 2.58% for φ. Those inversions illustrate that even without δ information, other TTI parameters, such as interface geometry, ε or tilted angle φ, still can be recovered properly. The parameter δ can be recovered by re-applying tomographic inversion or moveout analysis.

	True model			Inversion I			Inversion II	
	ε	φ	δ̄	ε	φ		ε	φ
Layer1	0.15	-14º	0.10	0.15	-14.079º		0.151	-12.559º
Layer2	0.10	22º	0.04	0.101	21.233º		0.095	26.584º
Layer3	0.14	1º	0.15	0.134	1.492º		0.156	-0.71º
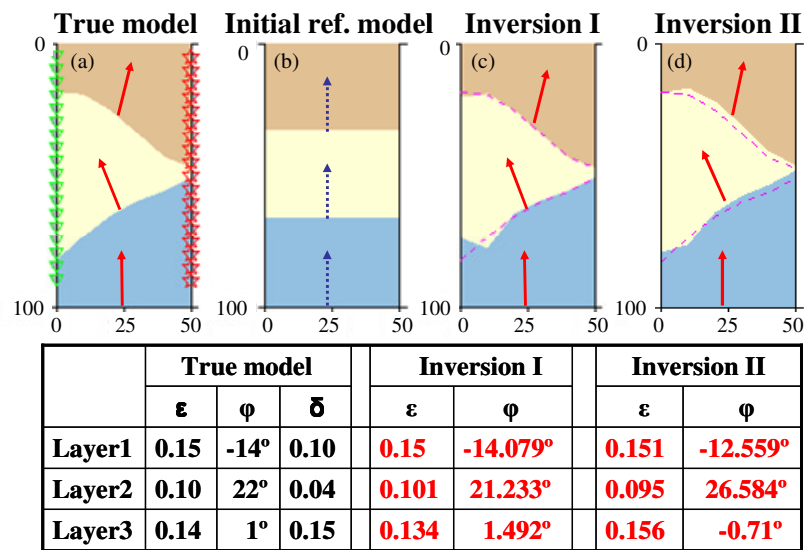
Figure 3-7: 2D TTI crosswell test. (a) True model; (b) Reference model; (c) The result of inversion I with δ of 0.1, 0.04, 0.15 in each layer; (d) The result of inversion II with δ of 0.0, 0.0, 0.0 in each layer. Red arrows represent true symmetry axes in (a) and inverted symmetry axes in (b) and (d). Blue arrows denote the initial vertical symmetry axes.

3.4.4 Crosswell anisotropic tomography in multi-layer media with 5% Gaussian noise

As same with previous tests, in this experiment, the 5% random Gauss noise is added into the input traveltime data to examine the reliability of anisotropic layer tomography. In this test, I invert for layer geometry, anisotropic parameter ε and tilted

angle φ of symmetry axis while parameter δ are constant during inversion process. From Figure (3-8), the inverted layer geometry still make the geologically sense with approximate structure and acceptable anisotropic parameters.

	True model	
	ε	$\varphi(°)$
Layer1	0.15	-14.0
Layer2	0.10	22.0
Layre3	0.14	1.0

	Inversion result	
	ε	$\varphi(°)$
Layer1	0.158	-17.27
Layer2	0.103	27.82
Layre3	0.124	-8.71
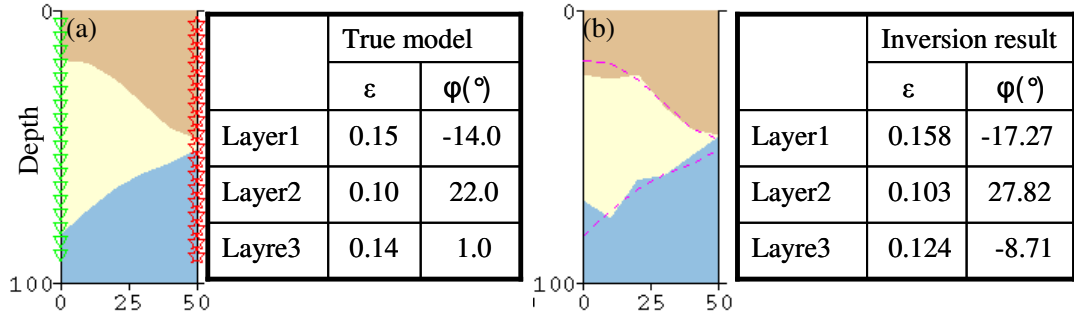
Figure 3-8: 2D Crosswell tomography by adding 5% Gaussian noise when inverting for layer geometry, ε and φ. (a) True model. (b) Inversion result. In this test, the inversion parameters are layer geometry, ε and tilted angle φ.

Figure (3-9) shows the inversion for the layer geometry, anisotropic parameter ε and δ together with 5% Gaussian noise in traveltime data when assuming tilted angle φ of symmetry axis is vertical. The difference between Figure (3-8) and Figure (3-9) is the inversion parameter δ instead of the tilted angle φ of the symmetry axes.

Crosswell acquisition geometry provides good ray coverage for detecting anisotropy, especially horizontal velocity. Large ray angle promise the ray path going through horizontally to increase the probability of inverting for anisotropic parameter ε successfully. However, crosswell acquisition geometry is not common acquisition geometry in industry because of high cost. Find a way to economically estimating structure properties is significant to reduce the exploitation expenses. Next chapter will give a discussion on how to build anisotropic velocity model with reasonable assumptions.

	True model				Inversion result	
	ε	δ			ε	δ
Layer1	0.15	0.10	Layer1		0.152	0.112
Layer2	0.10	0.04	Layer2		0.119	0.105
Layre3	0.14	0.15	Layre3		0.120	0.200
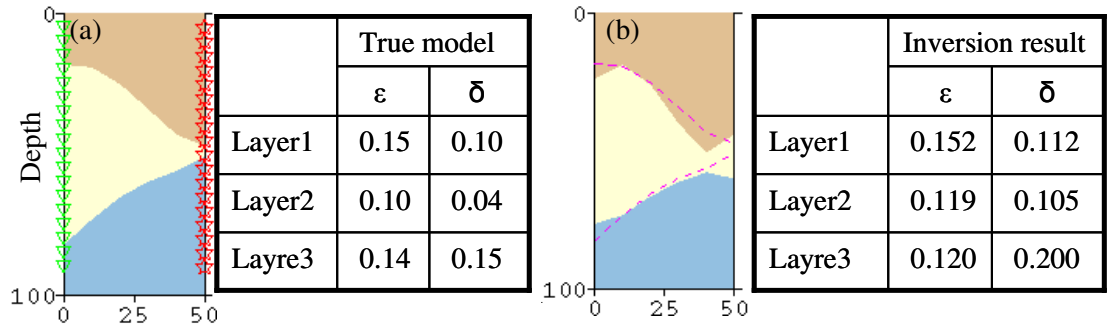
Figure 3-9: 2D Crosswell tomography by adding 5% Gaussian noise when inverting for layer geometry, ε and δ together. (a) True model. (b) Inversion result. In this test, the inversion parameters are layer geometry, ε and δ.

3.4.5 VSP anisotropic tomography in multi-layer media with noise-free data

VSP has been experimented as good acquisition geometry to detect anisotropy (*e.g.*, Slawinski et al., 2003; Maultzsch et al., 2007). A major challenge is to distinguish the effect of depth variation of velocity interfaces from that caused by anisotropy in the layer velocities, especially if only first arrivals are used. Simplifications like model with planar interface or fixed interface geometry have been implemented to help constrain the velocity models using VSP first arrivals. Here evaluate the inversion for the interface geometry and layered anisotropic parameters ε and δ using VSP first arrivals (Figure 3-10). The values of the true three-layer model are, from the top to bottom layers, the P-wave axial velocities of 2.0, 2.5, 3.0 km/s, and the tilted angles of 10°, -10°, 1° for the symmetry axes in these layers. Figure (3-10d) shows that the TTI parameters can be well resolved under an ideal situation with noise-free data, though the initial reference values differ much from the true model values. The details of each

inverted parameter are shown in Table (3-3). When ray coverage is improved, the results become more accurate.

True model

Raypath in true model

Initial Ref. Model

14th iteration
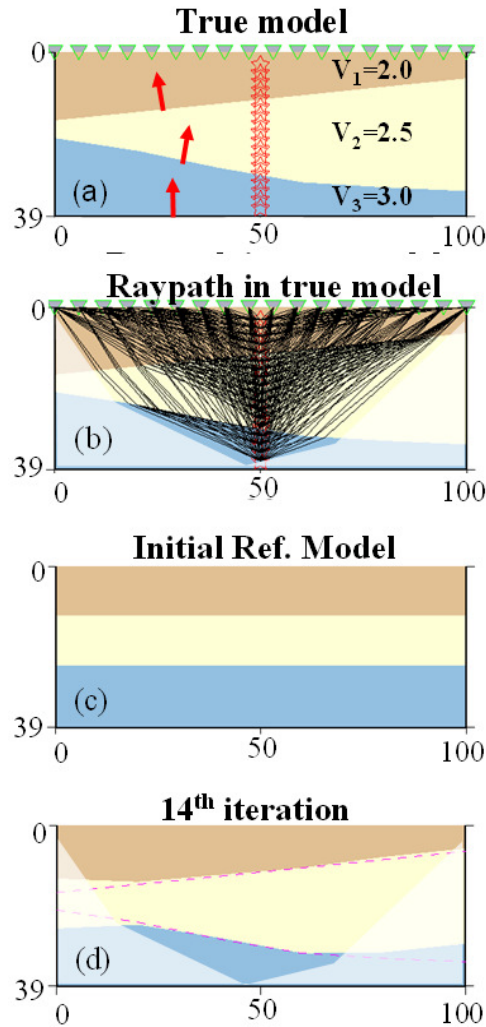
Figure 3-10: 2D layered TTI tomography by VSP first arrivals. (a) True TTI model and the distributions of sources (triangles) and receivers (stars). The arrows denote the tilted angles of symmetry in the layer anisotropic velocities. (b) TTI ray tracing in true model. (c) Initial reference model with isotropic assumptions. (d) Inverted model. The dash lines indicate the true interface geometry. The axial velocities are fixed during inversion process. In panels (b) and (d) the region outside ray coverage is lightened.

Table 3-3: 2D layered anisotropic parameter estimation using noise-free VSP first arrivals.

	True model		Initial reference model		Inverted model	
	ε	δ	ε	δ	ε	δ
Layer1	0.15	0.10	0.0	0.0	0.150	0.10
Layer2	0.10	0.04	0.0	0.0	0.093	0.038
Layer3	0.14	0.15	0.0	0.0	0.134	0.135

3.4.6 VSP anisotropic tomography in multi-layer media with 5% Gaussian noise

By adding 5% Gaussian noise in traveltime data, in this test, I invert for layer geometry, anisotropic parameters ε and δ together (Figure 3-11) when axial velocity is given. The inversion results show that in first layer, parameters ε and δ give good inverted value. However, because the layer geometry is deviated progressively from top layer down to bottom layer by introducing Gauss noise, ε and δ in third layer shows relatively large errors. It indicates that layer geometry can be more sensitively affected by traveltime data than ε and δ. However, for VSP acquisition geometry, check shot velocity is relatively easy to obtain and rough position of layer interface also can be guessed based on well-log data. The easiest case is to assume layer geometry is flat and use measured check shot velocity to invert for other parameters. Nevertheless, successfully estimating layer geometry and velocity together is still difficult. One solution may be to use prior geological information to constrain the variability of subsurface strata and give simple reference model.

| | True model | |
	ε	δ
Layer1	0.15	0.10
Layer2	0.10	0.04
Layre3	0.14	0.15

| | Inversion result | |
	ε	δ
Layer1	0.151	0.091
Layer2	0.153	0.011
Layre3	0.200	0.200
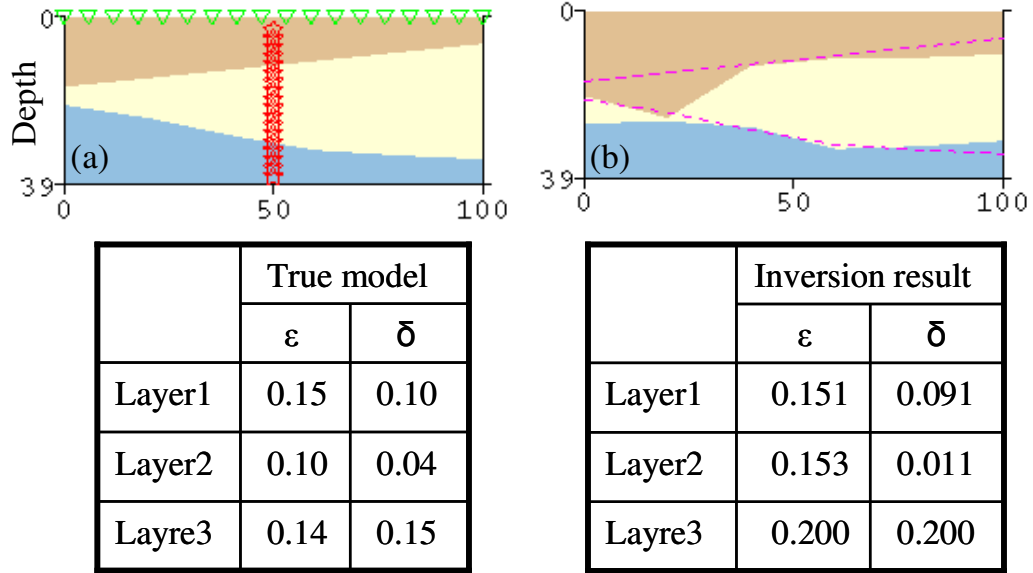
Figure 3-11: 2D VSP anisotropic layer tomography with 5% Gauss noise. (a) True model. (b) Inversion results.

3.5 NUMERICAL EXAMPLES OF ANISOTROPIC LAYERED TOMOGRAPHY IN 3D MEDIA

To examine the capability of the 3D layered traveltime tomography in TTI media, several synthetic true models are constructed with several deformable layers while each layer has different interval anisotropic parameters. The tilted symmetry axis is assumed to be perpendicular to bedding. The most critical for tomography in 3D media is ray path coverage. Sufficient ray path coverage from different directions will result in good quality of inversion result. However, any gaps or deficiencies in ray path coverage could affect the resolution of the tomographic results, and the most effective solution is to use wide-azimuth data with a wide spread of sources and receivers.

3.5.1 Anisotropic layer tomography by inverting for axial velocity, ε and δ

The first test shows a tomographic inversion for axial velocity $V_{p(0)}$, anisotropic parameter ε and δ using VSP first arrivals. The model is configured with 1004 sources on surface and 10 receivers placed in a vertical well (Figure 3-12). In this model, the ratio of offset over depth is almost close to five. This indicates that most rays travel horizontally. This provides good ray coverage for estimating horizontal velocity which is expressed by parameter ε. The interface geometry is fixed during inversion with tilted symmetry axis perpendicular to bedding. We use noise-free data to see how accurately the parameters can be obtained with poor initial guesses of the inversion parameters in 3D case (Table 3-4). After ten iterations, the results illustrate that these TTI parameters can be well resolved by new method under ideal situation. In Table (3-4), the red color denotes the reference model for tomographic inversion. The total twelve inversion variables are updated simultaneously in each iteration. As shown in Jiang and Zhou (2010), the resultant features are consistent with the sensitivity behaviors of the TTI kernels.

The inherent challenge of velocity modeling is the uncertainty of parameter estimation. TTI anisotropy is dominated in the tilted direction of primary thrusting, but counter thrusting and other minor deformation may reoriented or disrupt the effective symmetry axis. We analyze a test to invert for same parameters ($V_{p(0)}$, ε and δ) in VTI media by recorded first arrivals in TTI media. The interface geometry is given and symmetry axis is assumed to be vertical in each location. Table (3-5) shows the tomographic results. The quality of inversion result has been decreased slightly due to the assumption of VTI in TTI media. The inverted values with underline indicate that it may be not acceptable for depth imaging. The new ambiguity from tilted angle of symmetry axis can degrade the quality of anisotropic parameter building and lead to significant distortions in the image quality.
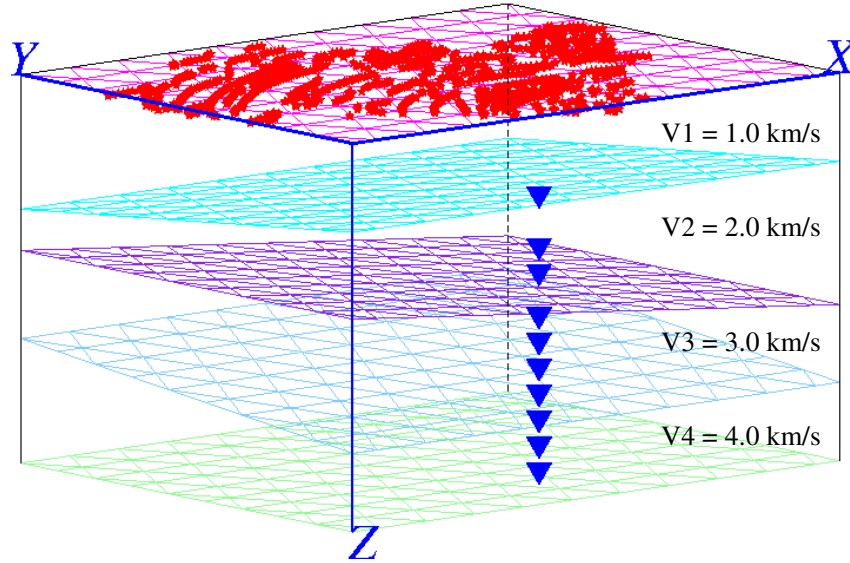
Figure 3-12: Model geometry and source and receiver distributions.

Table 3-4: Inversion results of 3D TTI tomography

	True (*Ref.*) Model				Inversion Result		
	$V_{p(0)}$ (km/s)	ε	δ		$V_{p(0)}$ (km/s)	ε	δ
Layer1	1.0 (*2.0*)	0.18 (*0.0*)	-0.11 (*0.0*)		1.000	0.177	-0.109
Layer2	2.0 (*3.0*)	0.14 (*0.0*)	-0.09 (*0.0*)		2.001	0.140	-0.091
Layer3	3.0 (*4.0*)	0.10 (*0.0*)	-0.07 (*0.0*)		3.019	0.095	-0.087
Layer4	4.0 (*5.0*)	0.07 (*0.0*)	-0.05 (*0.0*)		3.866	0.098	0.028

22

Table 3-5: 3D VTI tomography with TTI first arrival data

	True (*Ref.*) Model				Inversion Result		
	$V_{p(0)}$ (km/s)	ε	δ		$V_{p(0)}$ (km/s)	ε	δ
Layer1	1.0 (*2.0*)	0.18 (*0.0*)	-0.11 (*0.0*)		1.000	0.176	-0.105
Layer2	2.0 (*3.0*)	0.14 (*0.0*)	-0.09 (*0.0*)		1.998	0.140	-0.084
Layer3	3.0 (*4.0*)	0.10 (*0.0*)	-0.07 (*0.0*)		3.097	0.074	<u>-0.159</u>
Layer4	4.0 (*5.0*)	0.07 (*0.0*)	-0.05 (*0.0*)		3.588	<u>0.154</u>	<u>0.146</u>

3.5.2 Anisotropic layered tomography by inverting for layer geometry, ε and δ

In traditional cell or grid tomography, the inverted velocity is resolvable only at those places where there are a sufficient number of intersecting rays (Zhou, 2006). Poor ray coverage can lead to smear artifacts and poor resolution of velocity anomaly. Layered tomography is applicable where geological features such as weathering zone, salt bodies which can be represented easily by layers. In this test, I invert for thickness-vary layer geometry and anisotropic parameters ε and δ together with the assumption of tilted symmetry axis perpendicular to bedding. The layer geometry of synthetic true model is same with previous test but with ε = {0.18; 0.16; 0.14; 0.12} and δ = {-0.11; -0.13; -0.15; -0.17} from top to bottom layer. The initial reference model is given as planer model with zero anisotropy. Axial velocity in each layer is constant during inversion process. Figure (3-13) shows the reference model and inversion results by inverting for three thickness-varying layers and anisotropic parameter ε and δ together.

23

It shows parameter ε can be resolved under acceptable error range. However, δ shows that relatively high deviation. The reason is because the traveltime is depended on both layered kernels and anisotropic kernels, such as axial velocity, ε and δ. The layered kernels give strong influence on the calculated traveltime than kernels for δ. Because most ray travel horizontally, the kernels for ε provides relative large value and make ε "visible" during inversion process. On the whole, any gaps or deficiencies in raypath coverage could affect the resolution of tomographic results.

(a)

(b)
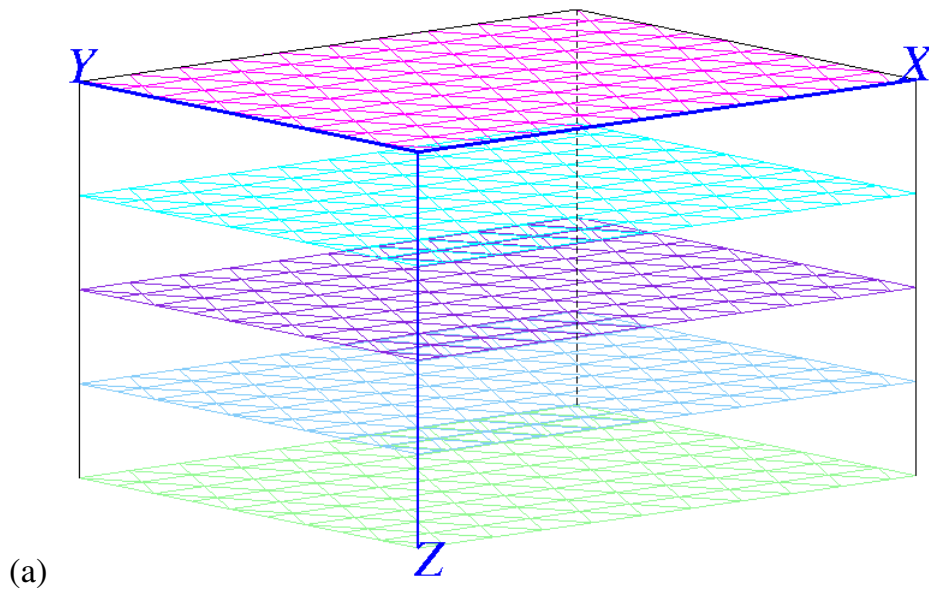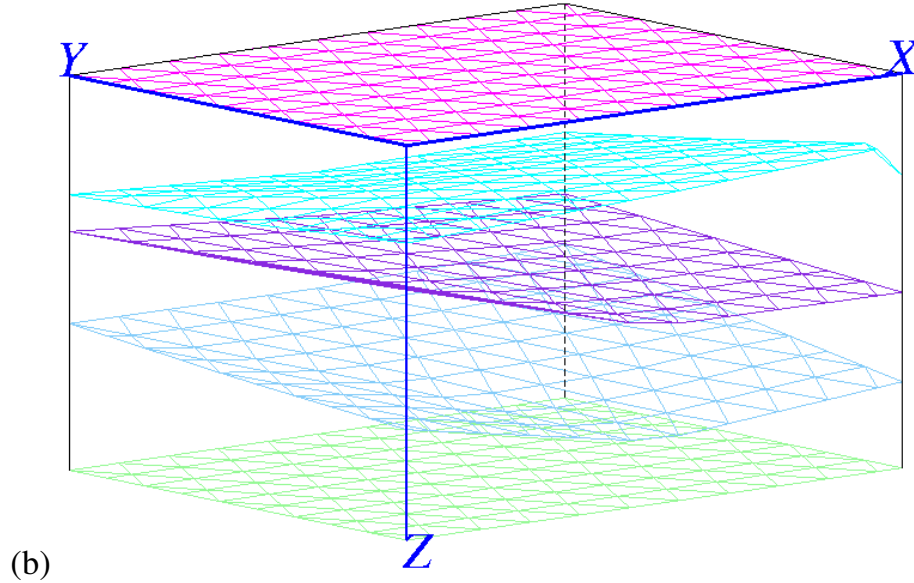
Figure 3-13: (a) Initial model; (b) Inversion result. In (b), the inverted ε are {0.167; 0.127; 0.109; 0.077} and inverted δ are {-0.163; -0.194; -0.113; -0.198} for the top to bottom layers. The parameter in true model are ε = {0.18; 0.16; 0.14; 0.12} and δ = {-0.11; -0.13; -0.15; -0.17}.

3.6 CHAPTER SUMMARY

Though good estimates of the anisotropic velocity structure will enhance the quality of depth imaging, results from many anisotropic depth-imaging projects are disappointing because estimating anisotropic parameters in depth domain depends on many elements. Sparse and irregular data acquisition, incomplete illumination of subsurface strata and erroneous data with low signal-to-noise ratios may result in incorrect estimates. In this study, an anisotropic layer tomography has been developed to estimate the anisotropic parameters in thickness-varying layered models. The traveltime equation leads to analytical kernels for different anisotropic parameters that illuminate the sensitivity of each anisotropic parameter with respect to various types of noise in traveltime data, including colored noise due to error in some of the model

25

parameters

In our model setup, each anisotropic layer has five types of parameters, the velocity along the symmetry axis, the thickness-varying interface, Thomsen's two anisotropic parameter ε and δ, and the tilted angle φ of the symmetry axes. The quality of the model parameterization and initial estimates of the model variables depends largely on the available geological and geophysical information. In the model parameterization process we shall always try to develop realistic but simple models that will help reduce the nonuniqueness in the model building process.

Although the synthetic tests in this chapter show good probability to invert for several anisotropic parameters using first arrivals, field data may bring more challenges. For example, irregular acquisition can limit the range of ray coverage and result in deficiencies in raypath direction, low signal to noise ratio will increase the difficulty and error in picking the first arrivals. Nevertheless, we expect the general trends of the relative resolvability of different anisotropic variables as revealed by several synthetic models will hold true. The inversion results need to be investigated with known geological understanding to verify that reliability.

CHAPTER 4: ERROR ANALYSIS OF ANISOTROPIC PARAMETER ESTIMATION BY A PRATICAL STRATEGY

4.1 INTRODUCTION

The difficulty in estimating the orientation and magnitude of the anisotropy in depth models affects the seismic imaging quality. In last chapter, a new TTI layered traveltime tomography is developed and testified successfully in several synthetic cases. However, inversions for all five anisotropic parameters together are impossible to provide reliable solution because each of parameters is controlled by the inversion results of other parameters. Therefore, it is necessary to find a practical strategy for estimating the parameter which has least sensitivity on the data errors (Jiang and Zhou, 2010). In this chapter, considering the varying ability to invert for different model parameters, I am searching for ways to invert only for some of the variables in such layered TTI models while fixing the other variables using their default values in particular acquisition geomotry. By applying the anisotropic layered traveltime tomography discussed in last chapter to a series of simple synthetic models, The analysis of the impacts of error in some of the model parameters on the inversion quality of the other parameters is discussed. Several experiments suggest that in crosswell acquisition geometry, axial velocity and ε should be considered for priority inversion variables, and consider δ as further inversion parameter when data coverage is sufficient. However, in VSP acquisition geometry, because most raypaths spread around 45°, δ can be considered as priority inversion parameter as well as axial velocity.

27

4.2 ERROR ANALYSIS OF ANISOTROPIC PARAMETER ESTIMATION

Considering the varying resolvability for different TTI model parameters in traveltime inversion, we want to evaluate the influence of error in each of the TTI parameters on the inverted result of other parameters. Because in many applications the data coverage may not allow for reliable inversion of all the TTI parameters, our evaluation may lead to a practical strategy to invert for the most resolvable TTI parameters. The evaluation is facilitated by applying the new tomography method to a series of simple synthetic models. Since the true model is known, the synthetic tests allow us quantifying the relative ability to recover each of the TTI parameters in the presence of error in other parameters.

To facilitate a meaningful comparison between the inversion errors of different model parameters, we define a normalized form of the error:

$$\text{Error} = \frac{m^{\text{true}} - m^{\text{pred}}}{m^{\text{range}}} \times 100\% \qquad (4\text{-}1)$$

where m^{true} stands for the true or observed value of the parameter such as the value of the true model in a synthetic test, m^{pred} stands for the predicted value from a model, such as the initial reference model, or the inverted value of the parameter. m^{range} stands for the possible range of the parameter in the inversion based on the known understanding (Thomsen, 1986; Tsvankin, 2001). In this study we assign a range of -20% to +20% for both ε and δ, hence the denominator in Equation (4-1) is 0.4 for ε and δ. Without loss of generality, in the synthetic models of this study the range for the axial velocity of each layer is from 1 to 4 km/s, and the range of the tilted angle of the symmetry axis is from -50° to +50°. Since Thomsen's parameters are represented

by the ratios of velocities and the size of errors for inherent anisotropy scale, the parameter m^{range} is specified to quantify how sensitive of each parameter is affected by errors from other parameters. In this study, we use Equation (4-1) to quantify errors in the initially referenced model parameters, and we also use the absolute value of Equation (4-1) to quantify the impact of errors in each parameter on the inversion results of other parameters.

4.2.1 Error analysis of parameter estimation in a 2D simple TTI model

I start using a simplest case of a 2D TTI tomography in a block model with analyzing different anisotropic parameters. Those two model shown in Figure (4-1) but they are exactly same with Figure (3-7).
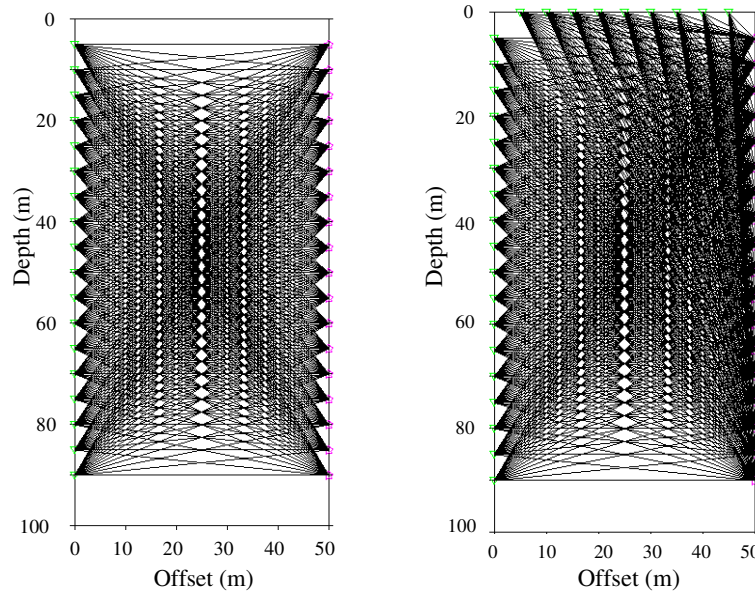
Figure 4-1: Two seismic recording geometries and their relative raypaths in a single block model. (a) Crosswell geometry. (b) Crosswell plus VSP geometry. The triangle indicates the source, and the star indicates the receiver.

Though δ is one of the significant parameters describing velocity anisotropy (*e.g.*, Thomsen, 1986; Berryman et al., 1999), it is questionable weather δ can be reliably inverted using conventional acquisition geometry, such as crosswell acquisition geometry. Here I analyze the impact of errors in δ on the inversion of other parameters by TTI layered traveltime tomography. By setting δ to zero value in the true model but using different δ values in the initial reference model, we invert for the axial velocity, ε, and the tilted angle φ together. The error of δ is the difference between its values in the true model and the reference model, and this behaves as a defined noise to the inversion of the other model parameters. Table (4-1) and (Table 4-2) show the statistic errors from tests of the TTI traveltime tomography using different levels of the noise in δ. Even when the noise in δ approaches from 10% to 20%, it causes only 1.1% error in the inverted value for the axial velocity, 0.8% error in the inverted value for ε, and 0.6% error in the inverted value for the tilted angle φ in the case of crosswell recording geometry. In the case of crosswell plus VSP recording geometry, the inverted error is reduced to 0.7% in the axial velocity, 0.5% in the ε value, and 0.6% in the tilted angle φ. These results indicate that the error in δ may not bring large impact on the inversion results of other parameters in such cases with wide angle coverage of ray paths.

The symmetry axes of the TTI anisotropy may be altered due to thrusting and other deformations. Since I assume an variable symmetry axis for each model layer, additional errors in the symmetry axis may occur. Here I consider the impact of noises in the tilted angle φ of the symmetry axis on the inversion results of other parameters. We assign 10% error in the tilted angle φ and invert for the axial velocity, ε and δ together. Using the crosswell recording geometry, this 10% noise in the tilted angle φ can cause 1.7% error in the inverted axial velocity, 3.8% error in the inverted ε, and

18.3% error in the inverted δ. Using the crosswell plus VSP geometry, due to the improved ray coverage with more ray paths along 45° angle (for δ) and near-90° angle (for ε), 10% noise in the tilted angle φ caused only 0.2% error in the inverted axial velocity, 0.8% error in the inverted ε value, and especially 2.5% error in the inverted δ value which has been significantly decreased. This synthetic tests suggest that the axial velocity and ε may not be largely affected by the errors from tilted angle of symmetry axis or δ, they could be considered as primary parameters to estimate with crosswell acquisition geometry. Since δ brings less error on estimating other parameters and it is only sensitive when ray angles are around 45°, δ may be estimated last for crosswell geometry.

Table 4-1: Inversion errors using four levels of noise in δ with the crosswell geometry.

δ in the true model	δ in the initial reference model	Given error of δ	Inversion errors of other parameters		
			V_{p0}	ε	φ
0.0	0.10	- 25.0%	1.1%	0.8%	0.6%
	0.05	- 12.5%	0.5%	0.5%	0.8%
	- 0.05	12.5%	0.5%	0.5%	0.2%
	- 0.10	25.0%	1.1%	1.0%	0.5%

Table 4-2: Inversion errors using four levels of noise in δ with the crosswell plus VSP geometry.

δ in the true model	δ in the initial reference model	Given error of δ	Inversion errors of other parameters		
			V_{p0}	ε	φ
0.0	0.10	- 25.0%	0.7%	0.5%	0.6%
	0.05	- 12.5%	0.3%	0.3%	0.5%
	- 0.05	12.5%	0.3%	0.3%	0.6%
	- 0.10	25.0%	0.4%	0.5%	0.8%

4.2.2 Error analysis of parameter estimation in 2D layered TTI model

To quantify the effects of errors in the TTI parameters, we repeated the layered tomography inversion which has same layer geometry with Figure (3-10) for ε and δ under different assumptions for the tilted angle of the symmetry axes, but using the known layer geometry and axial velocities. The true ε and δ are set to $\varepsilon = \{0.18; 0.14; 0.12\}$ and $\delta = \{0.17; 0.13; 0.09\}$ from top to bottom layer. The error in the tilted angle of the symmetry axes can be considered as pre-defined noise in the data space. The true model is the same as in Figure (3-11) with the tilted angle is 20°, -20°, 0° from the top to the bottom layers (Figure 4-2). The error of φ increases from 0° (VTI) to 10% for the first two layers in the reference models of four synthetic tests. Table (4-3) shows the influence of the error in φ on the inverted results of parameters ε and δ, where each inverted error is the average of the inverted errors of the three model layers. 10% error in φ brought 4% average error in the inverted ε value, but up to 12% average error in the inverted δ value. The large error is disappointed because from general sense δ should be easier to resolve than ε in VSP setting. However, this test illustrates that tilted angle of symmetry axis could give large impact for inverting anisotropic parameter. Simply treating media as VTI can simplify the processing step and save computation time either in tomography or depth migration, but bring more errors on final results.
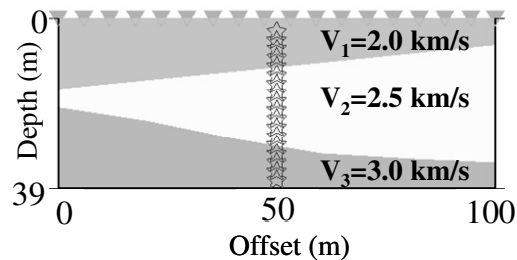
Figure 4-2: Velocity model for testing of error analysis.

Table 4-3: The influence of noise in φ on the inverted values of ε and δ.

φ$_{true}$ [°]	φ$_{init}$ [°]	Given error of φ	Inversion errors of other parameters	
			ε	δ
{20; -20; 0}	20; -20; 0	0%	0.0%	0.0%
	15; -15; 0	5%	2.1%	9.5%
	10; -10; 0	10%	3.8%	12.5%

To estimating anisotropic parameter, different acquisition offsets can provide different aspects (Yuan et al., 2002). Generally, shot-spread offset, such as, the offset equals to the depth of deepest receiver, is used for determining check shot velocity, or axial velocity. Intermediate offset is good for determining moveout velocity which is $V_{moueout}=V_{p0}(1+2\delta)$. Therefore parameter δ could be iteratively resolved. Because parameter δ is couple with axial velocity, any errors from measurement on axial velocity V_{p0} will result in instability for building δ model. Long-offset (the ratio of offset verse depth is greater than four) is good for estimating parameter ε since most ray will travel horizontally. In either case, the discussion of analytical kernels in Chapter 3 declares that axial velocity will be most resolvable and most-error tolerant parameter to be estimate as priority parameter. The errors in axial velocity are considered as noises in the data space. After tenth iteration of tomography, we notice that even 5% errors in axial velocity will bring more than 10% errors for ε and more than 15% errors for δ. This experiments shows that axial velocity could play the most important role in estimating any other parameters. The comparison between different kernels on varying ray angles (Fig 3-1) shows that even at ray angle 45°, where the peak magnitude of kernel δ presents, the peak magnitude of axial velocity is still five to six times greater than δ. Either reason will make inverting for δ difficult. However, in VSP acquisition geometry, velocity along well-bore are typically known and can be

measured directly. This provides good opportunity to estimate ε and δ together from layered traveltime tomography.

4.2.3 Error analysis of parameter estimation in 3D layered TTI media

To examine the error effects on the inversion result by 3D TTI inversion, a synthetic model is constructed with four TTI layers and each layer has different anisotropic parameters. The tilted symmetry axis is assumed to be perpendicular to bedding. Figure (4-4) shows raypaths from many surface sources to a receiver in the wellbore for both an isotropic model and a TTI model examined in this test. Table (4-4) shows the results of layered anisotropic estimation by inverting ε and δ simultaneously. The large number of 1004 sources from different azimuth directions improves the ray coverage. The average inversion error for ε is 0.5% and for δ is 0.61% which are in same error level. The minor differences between the true parameters and estimated parameters are expected and are caused primarily by deficiencies in ray coverage along certain angles. Although this test shows the good capability to recovery the layered parameters, any incomplete ray coverage will make it very difficult to recover all the anisotropic parameters. In this case, because of large offset (the ratio of offset verse depth is close to five), parameter ε and δ can be resolved accurately.
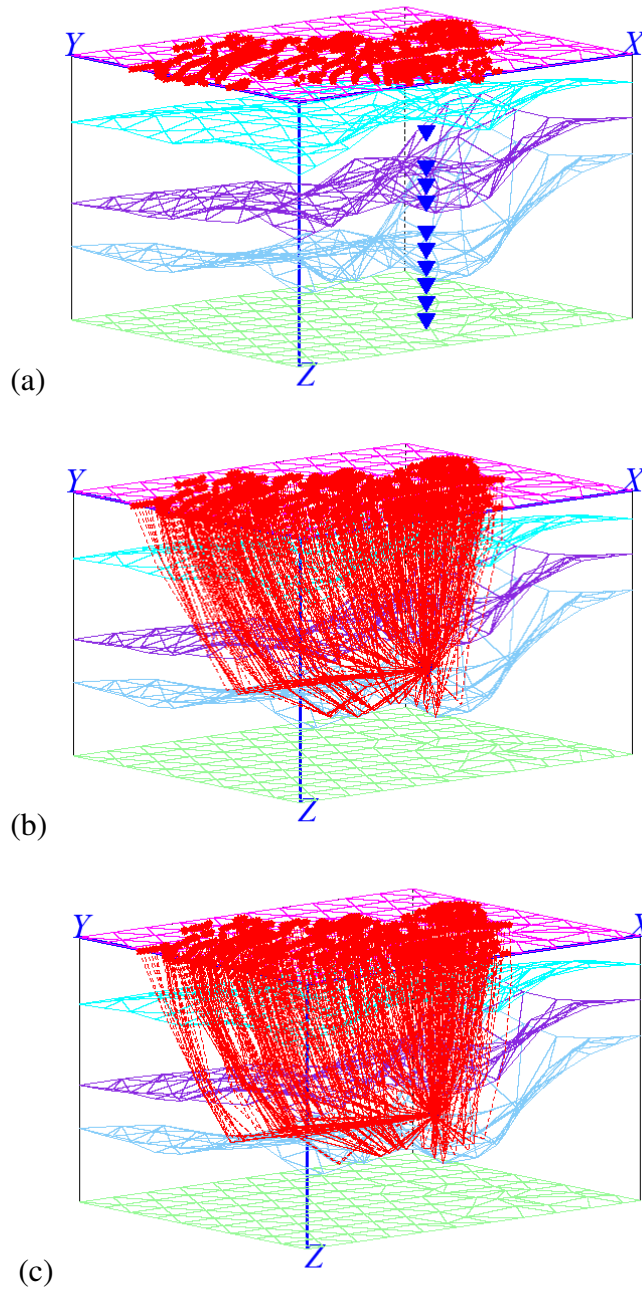
Figure 4-4: 3D ray tracing in isotropic and TTI media. (a) Model geometry and distributions of surface sources (stars) and in-wellbore receivers (solid triangles). (b) Raypaths (dashed lines) in isotropic reference model from one receiver located in the third layer. (c) Raypaths in synthetic TTI model with assumption of tilted symmetry axis perpendicular to layer interface.

Table 4-4: 3D layered anisotropic parameter estimation by inverting ε and δ together.

	True model		Reference model		Inverted model	
	ε	δ	ε	δ	ε	δ
Layer1	0.12	0.03	0.0	0.0	0.119	0.029
Layer2	0.14	0.05	0.0	0.0	0.140	0.057
Layer3	0.16	0.07	0.0	0.0	0.163	0.065
Layer4	0.18	0.09	0.0	0.0	0.180	0.091

How the errors of layer geometry effect on the different inversion parameters? The following experiment testifies that the dependence of inversion parameter ε and δ on the layer geometry. Figure (4-5) shows the tomographic inversion for ε and δ when layer geometry in reference model is deviated from true model. In this test, the second layer is moved up and the third layer is moved down about 10% of the total depth. Each layer has constant velocity and the tilted angle of symmetry axis is perpendicular to layer bedding in each location.

(a) True model   (b) Reference model
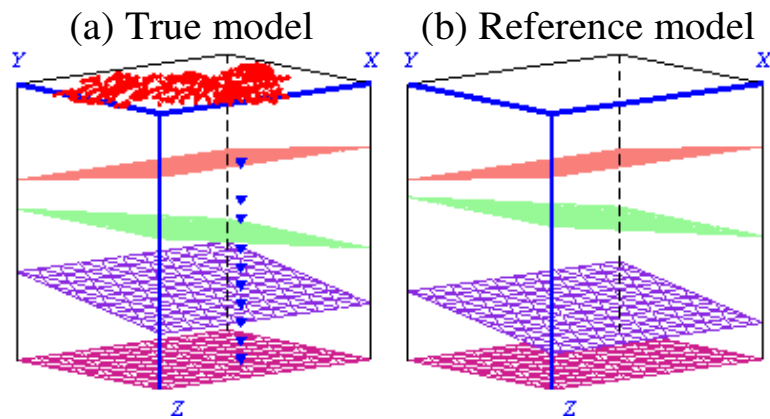
Figure 4-5: The different layer geometry setups. (a) True model; (b) Reference model. In (b), the second layer is moved up and third layer is moved down about 10% of vertical depth. The first layer is same with true model.

Table 4-5: The inversion result with deviated layer geometry.

	True model		Reference model		Inverted model	
	ε	δ	ε	δ	ε	δ
Layer1	0.18	-0.11	0.0	0.0	0.192	-0.123
Layer2	0.14	-0.09	0.0	0.0	0.141	-0.173
Layer3	0.10	-0.07	0.0	0.0	0.037	0.170
Layer4	0.07	-0.05	0.0	0.0	0.089	-0.200

From Table (4-5), the errors in layer geometry bring large influence on parameter δ. This indicates that to solve parameter δ accurately, good assumption of subsurface structure from well log data is needed. Xiao et al. (2005) denotes that the accuracy of estimated anisotropic parameter depends not only on the accuracy of the picked NMO velocity but also on the value of $(\varepsilon-\delta)$. The smaller the value of $(\varepsilon-\delta)$ and the value of ε, the higher the accuracy of estimated δ. Therefore, the more stable solution maybe inverted for elliptical anisotropic parameter $\eta=(\varepsilon-\delta)/(1+2\varepsilon)$, the derivation of analytical kernels for η is still an ongoing project.

4.3 A PRACTICAL STRATEGY FOR ANISOTROPIC PARAMETER ESTIMATION

The above experiments show the different sensitivities of each anisotropic parameter on the colored-noise in different acquisition geometries. According to the analyses of statistic errors in different acquisition geometry, the strategy for determining anisotropic parameter can be summarized in Figure 4-6. The resolvability can be quite different depending on acquisition geometry and offsets. To obtain best reliability of building velocity model, a prior information from previous research or experience should guide to right direction.
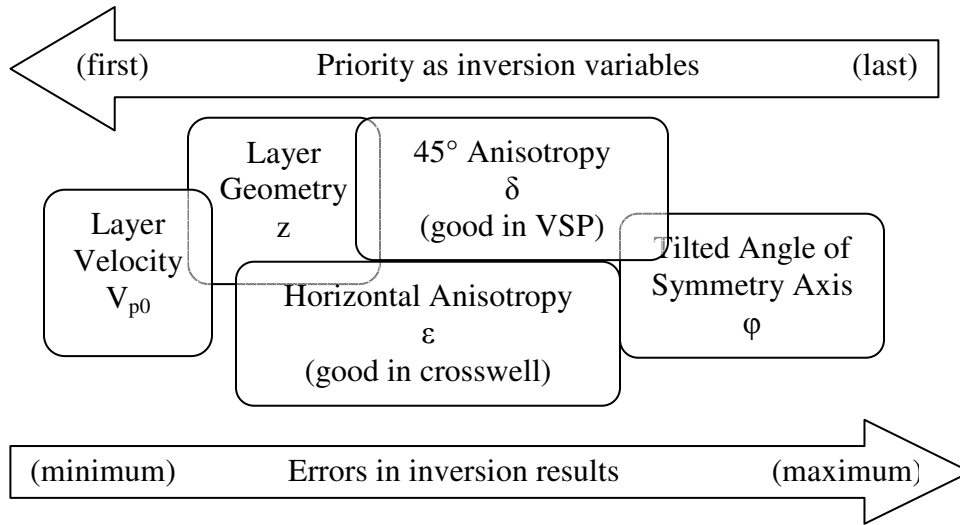
Figure 4-6: A general workflow developed for layered anisotropic parameter estimation.

4.4 CHAPTER SUMMARY

Our analysis indicates that inversion for the tilted symmetry axis of TTI models creates a new ambiguity in anisotropic seismic tomography. The error in the assumptions that the symmetry axis is vertical (VTI) or horizontal (HTI) may degrade the quality of the parameter estimation for TTI media and lead to significant distortions in the image quality. Error as noise in the layer velocity plays a critical role governing the qualities of overall inversion results. The assumption of 5% error in velocity will bring more than 10% error in the inverted ε value and 15% error in the inverted δ value that is unacceptable. Because δ is highly couple with axial velocity, any changes in axial velocity will magnify the errors shown in δ. In crosswell acquisition geometry, the inversion of δ is particularly unstable in comparison with that for the axial velocity and ε. However, an error in δ does not bring significant error on the inverted values of the velocity and ε in crosswell case which provides near-90° ray path and make ε is most sensitive with traveltime perturbation. Therefore,

38

assuming δ as constant value is a reasonable decision when no information is available about the type of the anisotropy in crosswell geometry. In VSP case, determining ε and δ become more difficult because those parameters are not only depending on the ray path coverage, but also on the derived check-shot velocity, predicted layer geometry, even different offsets. In either acquisition geometry, any gaps or deficiencies in raypath coverage could affect the resolution of the tomographic results, and the most effective solution is to use wide-azimuth data with a wide spread of sources and receivers. The choices on the complexity level of the anisotropic depth model and what parameters to invert depend on the available data quality, coverage, and study objectives.

CHAPTER 5: ANISOTROPIC PARAMETER ANALYSIS BY PRESTACK REVERSE TIME MIGRATION

5.1 INTRODUCTION

Reverse time migration (RTM) has been successfully applied to produce high images in recent years. It propagates source wavefield forward in time and the receiver wavefield backward to image the subsurface reflector (*e.g.*: Baysal et al, 1983; McMechan, 1983; Whitmore, 1983). By using the two-way acoustic wave equation, RTM has no dip limitation. Also, it naturally takes into account both down-going and up-going waves and thus enables imaging of the turning waves and prism waves that are able to enhance the image of steep salt flank and other steeply dipping events with complex structures.

Conventional isotropic RTM produces erroneous images and generates misposition of the dipping events in TI media. When multi-component data are available, the elastic RTM seems to be a proper treatment in anisotropic media. However, separating anisotropic wavefield into different wave modes for reflector imaging is difficult in terms of accuracy and efficiency. Rather than solving the complicated anisotropic elastic wave equation, many researchers focus on developing simple two-way wave equation to perform acoustic anisotropic RTM of pressure data (Alkhalifah, 1998).

In this chapter, the image results of RTM generated by different assumptions of anisotropic parameters are discussed. Different estimations will influence the image results and bring difficulties on seismic interpretation. The conclusions of the impacts

of each anisotropic parameter on RTM agree with the conclusions from the error analysis by traveltime tomography. Each parameter will bring different impacts on migration results as well as on traveltime tomography.

5.2 IMPLEMENTATION OF REVERSE TIME MIGRATION IN ANISOTROPIC MEDIA

The regular procedure of anisotropic RTM is listed as:

1. Estimating anisotropic parameters from surface data or well data;

2. Preprocessing of seismic data;

3. Forward wave propagation from source;

4. Backward wave propagation from receivers;

5. Apply the zero-lag cross correlation imaging conditions;

6. Stacked partial migrated results into final whole images.

In this chapter, the influence of anisotropic parameters on migration results is analyzed. Each migration experiment follows the above processing procedure and shows some common issues on reverse time migration.

5.2.1 Synthetic examples of prestack reverse time migration in anisotropic media

To verify the anisotropic RTM algorithm for parameter analysis, several examples are conducted. Figure (5-1) shows a velocity model in TTI media. Following the processing step mentioned above and two-way acoustic wave equation (2-7), by

crosscorrelating between forward wavefield and backward wavefield (Figure 5-2), the
RTM result is generated and showed on Figure (5-3).
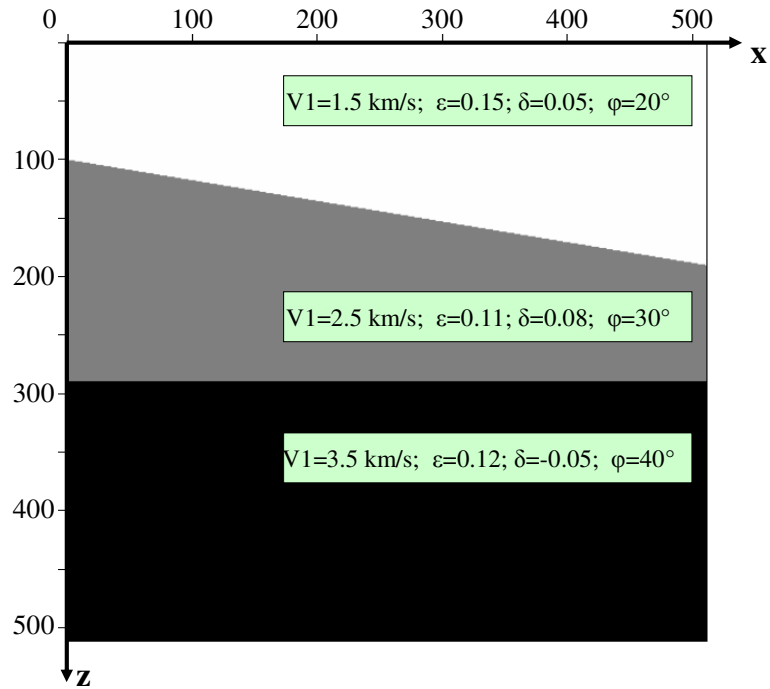
Figure 5-1: TTI velocity model.
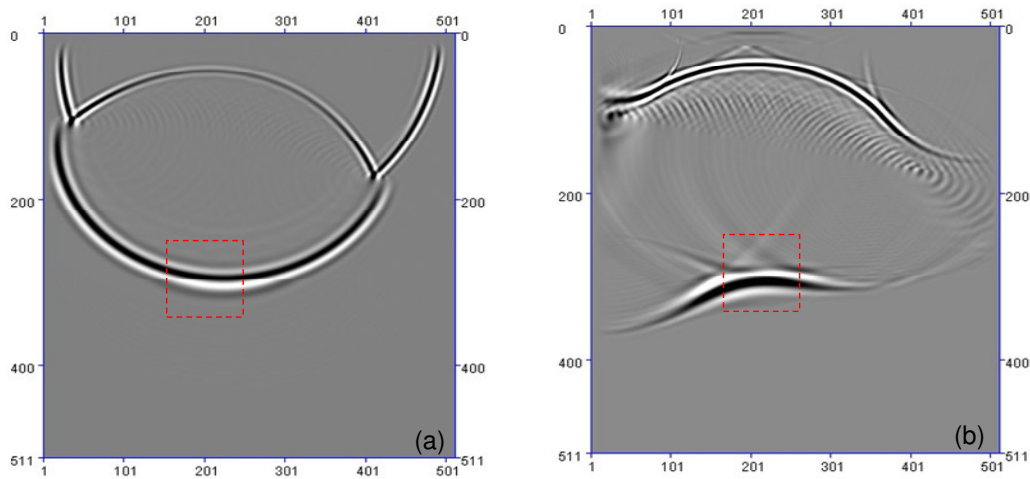
Figure 5-2: Crosscorrelation between forward wavefield and backward wavefield. (a)
forward wavefield at time t; (b) backward wavefield at reversed time (ttotal-t). The red
box shows the location of the possible images could be formed.
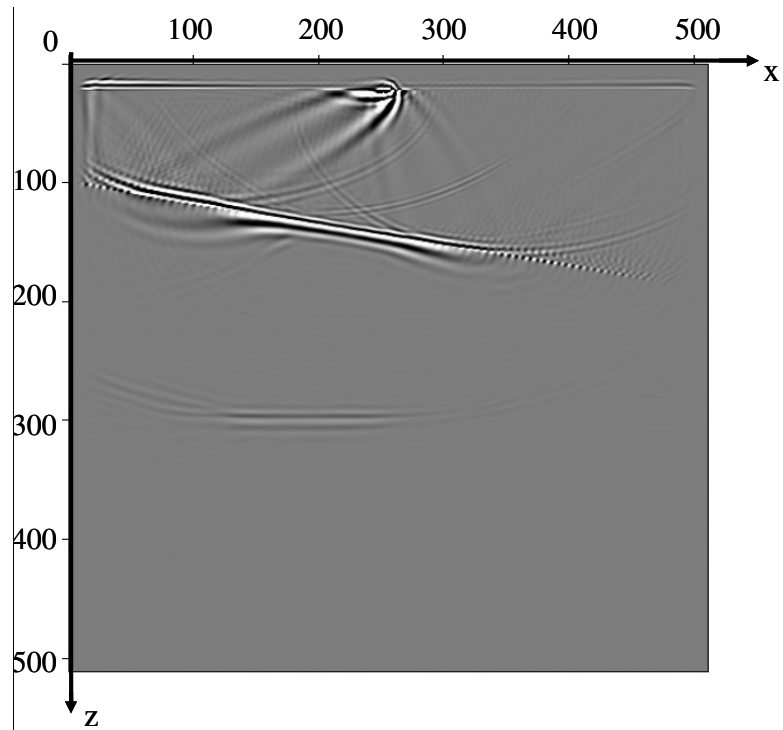
Figure 5-3: A single shot image generated by TTI RTM.

Anisotropy will result in errors of subsurface strata and the reflection point could be imaged away from its true location. The following test shows an isotropic RTM implemented in a TTI media (Figure 5-4). In isotropic RTM, the first dipping reflector is imaged at shallower location and becomes curved at right side. It may bring difficulties on seismic interpretation if salt structure or reservoir presented.
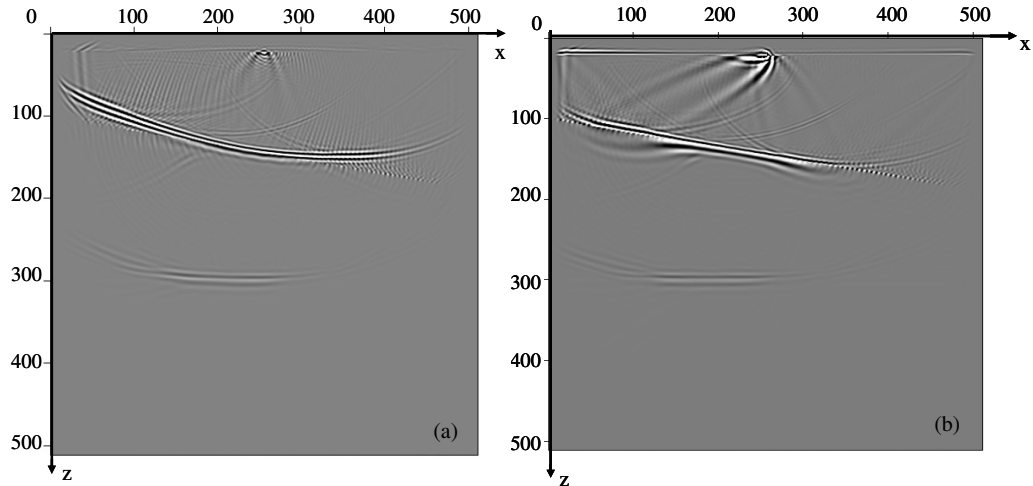
Figure 5-4: The comparison between isotropic RTM and anisotropic RTM. (a) Isotropic RTM; (b) Anisotropic RTM.

5.2.2 The analysis of influence of anisotropic parameters by prestack reverse time migration

In Chapter 4, a practical strategy for anisotropic parameter estimation is proposed. The different assumptions to estimate anisotropic parameter play an important role on the quality of migration process. In reality, it is impossible to construct all anisotropic parameters simultaneously and accurately, it is necessary to quantitatively analyze the influence of different parameters on the migration results. In the following, several experiments are conducted with different assumptions on anisotropic parameters. Each parameter brings different influences on the images, such as, without known the accurate model of anisotropic parameter δ, the imaging result still reasonable compared with the results migrated by the model if without known accurate ε. This is identical with the conclusions of anisotropy traveltime tomography in last chapter. The tilted angle of symmetry axis affects the reflector depth on steep dip boundary, but does not have large impact on flatten subsurface strata. Figure (5-5) shows a synthetic anisotropic velocity model and its migration results. The anisotropic parameters in each layer are shown on Table (5-1). The final image is stacked by partial images

generated from five common shot gathers. We notice that near the source locations, each source generates similar artifacts along receiver line. This is because the imaging condition of nature RTM algorithm between forward wavefield and backward wavefield, but it would not affect the image on the reflection strata.
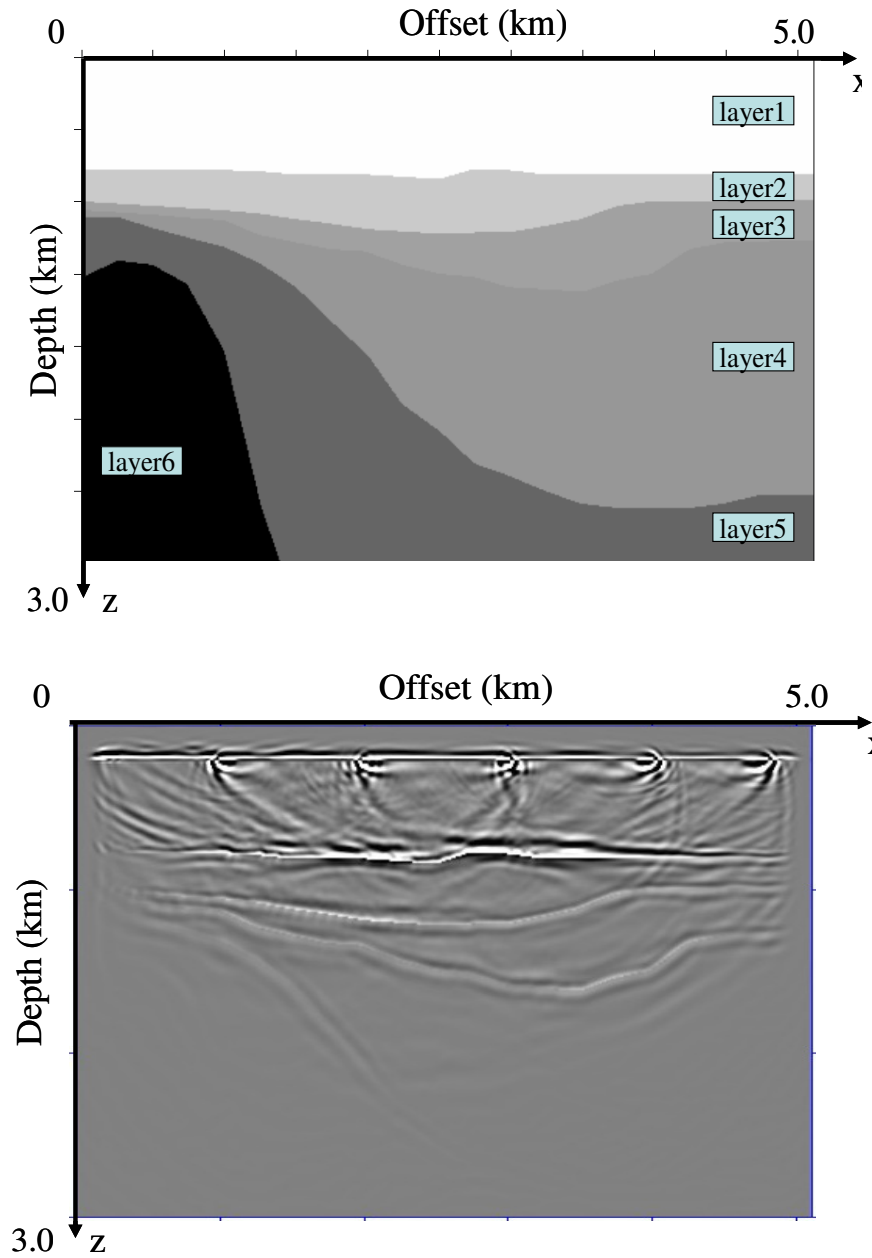
Figure 5-5: (a) Synthetic anisotropic velocity model. (b) Depth image results stacked by five partial images.

Table 5-1: Anisotropic parameters in true model

	Velocity (km/s)	ε	δ	$\varphi(°)$
Layer1	1.5	0.13	0.13	0
Layer2	2.0	0.17	0.12	10
Layer3	2.5	0.15	-0.15	15
Layer4	3.0	0.19	-0.13	30
Layer5	3.5	0.18	-0.10	50
Layer6	4.0	0.0	0.0	0

5.2.2.1 The influence of δ on image quality

The first test is to assume anisotropic parameter δ equal to zero in the model (Figure 5-5), however, other parameters are same with true model. The shot gathers are generated with true anisotropic parameters. Figure (5-6) shows the partial image result. From Figure (5-6), even δ is inaccurate, the image quality displays good coherence with true model. The nature of δ describes that how the wave propagation deviates away from vertical direction. Therefore, δ will take critical effect when imaging for steeply dip reflector. Because δ is hard to estimate especially from surface data, we may assume δ as zero to start migration process first, the final result can be re-migrated if other information, such as well control, is available.

(a)

(b)
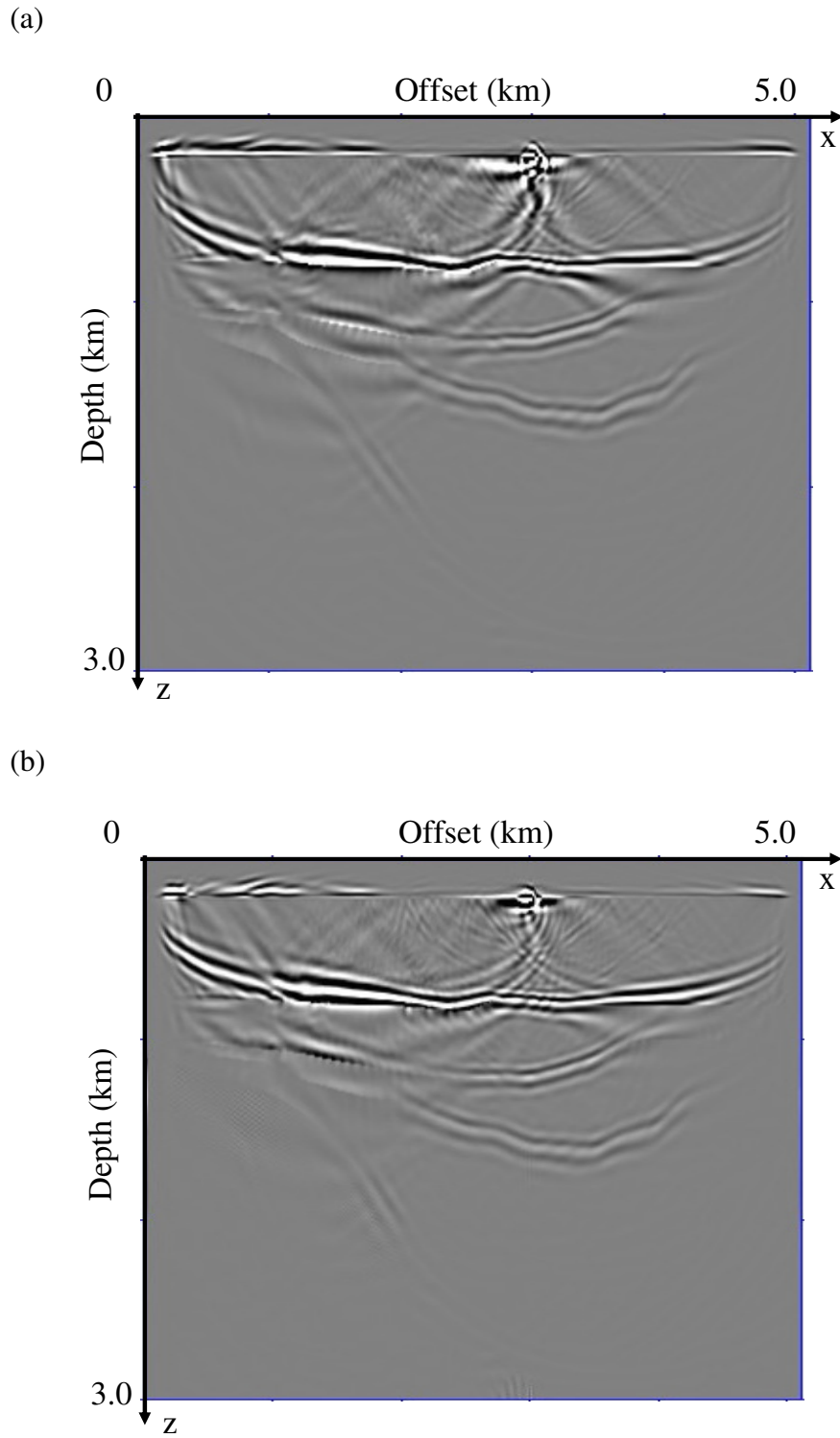
Figure 5-6: The influence of δ on image result. (a) Depth image with all true
parameters; (b) Depth image when δ = 0.

5.2.2.2 The influence of ε on image quality

Figure (5-7) shows RTM results if ε is assumed to be zero. Unlike parameter δ, predictive ε value brings large errors on the image result. The nature of ε illustrates that the fractional velocity difference between horizontal and vertical direction. Ignoring ε means the velocity field will be treated as same at horizontal and vertical direction, which becomes near-isotropic. In this view of point, ε plays a very important role on both traveltime tomography and migration process. It should be considered as priority parameter to get resolved.

(a)
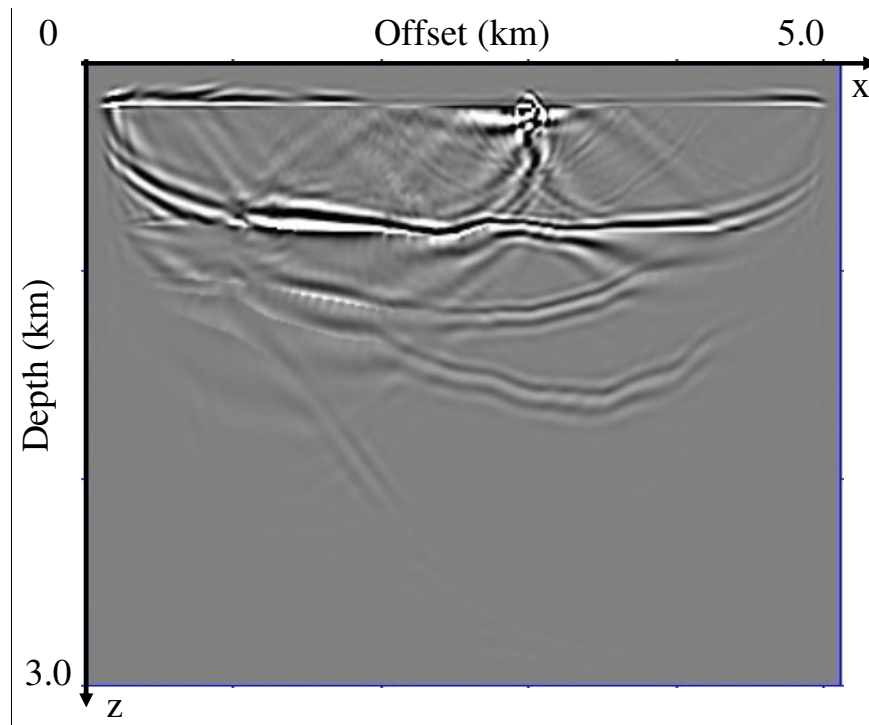
(b)
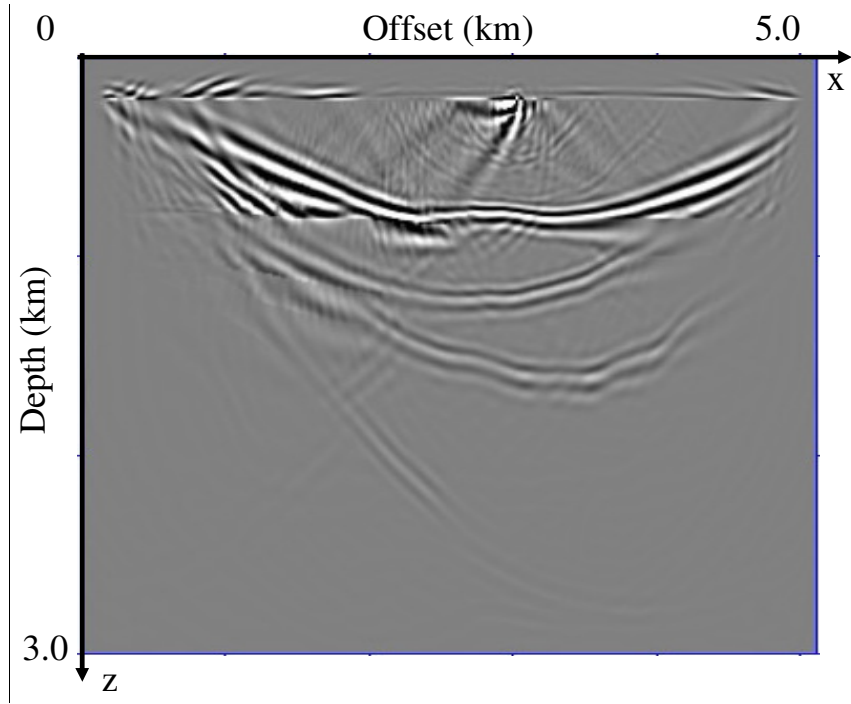
(c)
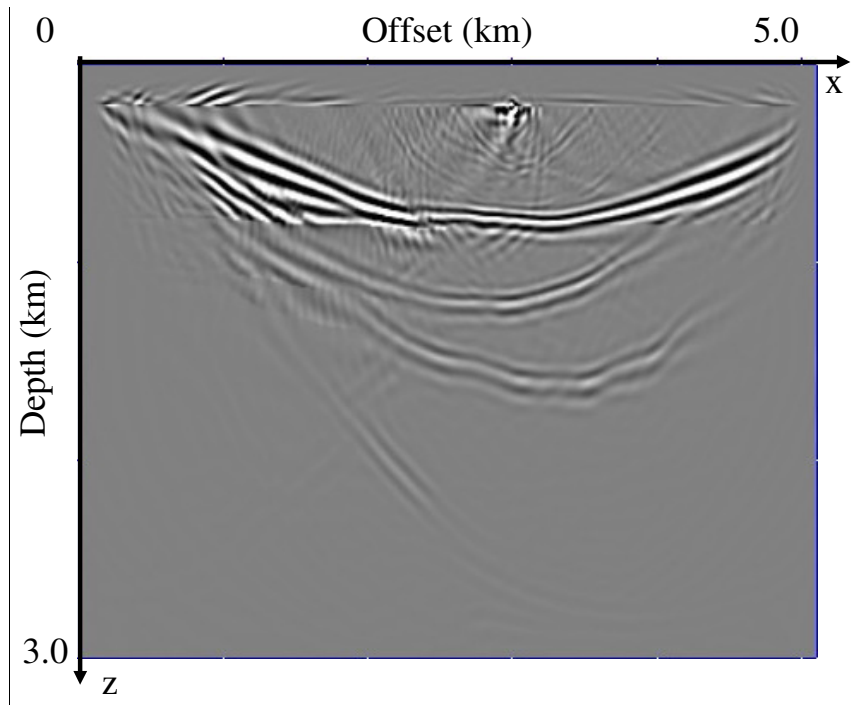
Figure 5-7: The influence of ε on image equality. (a) Anisotropic image with all true parameters; (b) Anisotropic image when ε = 0; (c) Isotropic image.

5.2.2.3 The influence of tilted symmetry axis on image quality

When ignoring tilted angle φ, TTI media will become VTI media. The tilted angle φ controls the fast direction of wave propagations, ignoring it will result in the deviation on the vertical depth and dipping angle of imaged reflectors. Figure (5-8) shows the two depth images with different assumptions of tilted angle φ. The two cross points point out that if ignoring tilted angle of symmetry axis in anisotropic media, the reflector point will be imaged away from its true location and the final reflector will display errors from true location of subsurface strata.

(a)
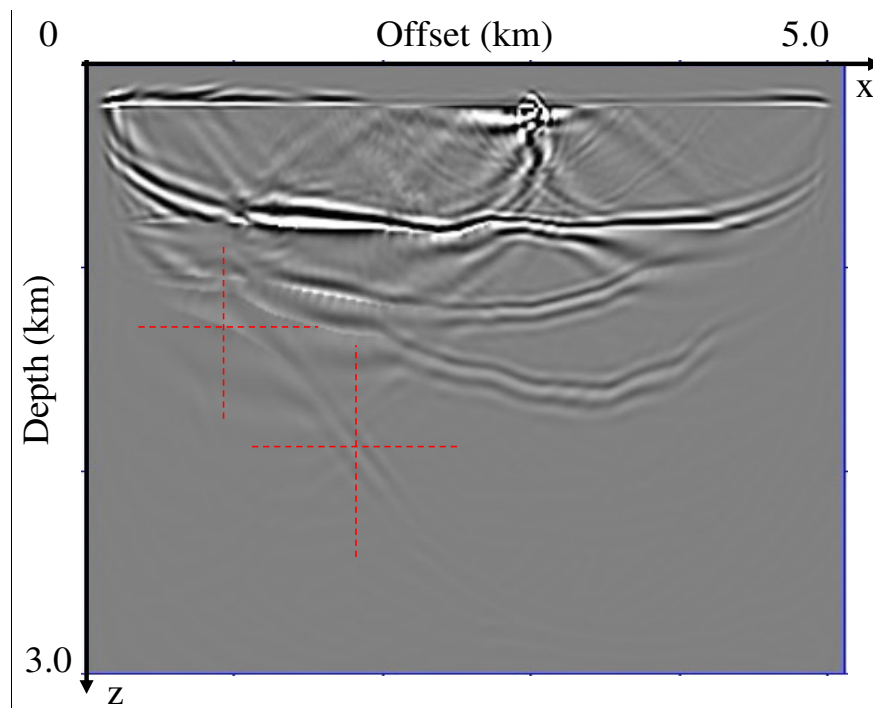
(b)
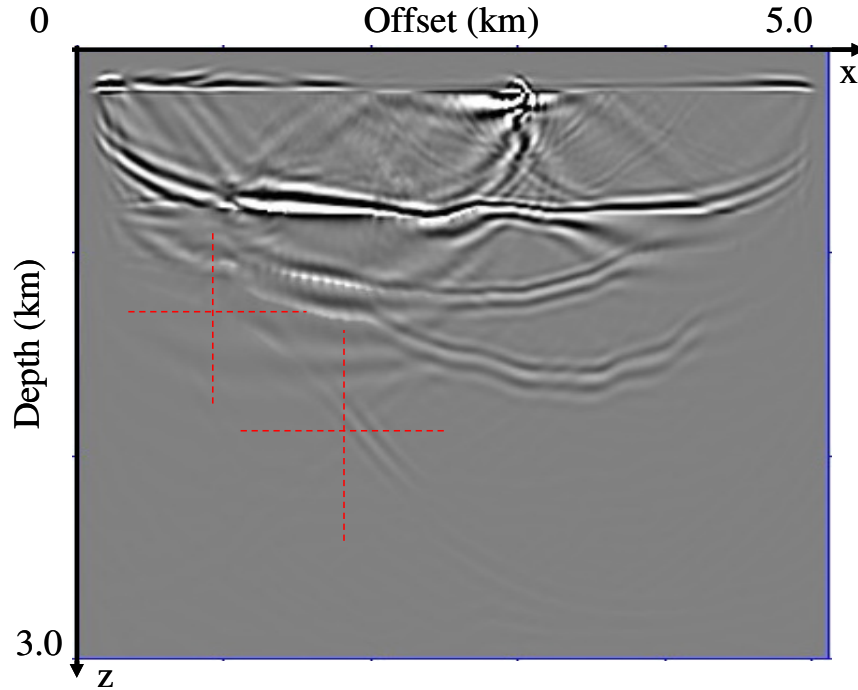
Figure 5-8: The influence of tilted symmetry axis on image quality. (a) Depth image with TTI assumption; (b) Depth image with VTI assumption. The dashed cross-lines marked the difference from two different migration algorithms. The most influenced area by tilted symmetry axis is the steeply dipped reflector, the flatten area is hardly affected by tilted symmetry axis.

5.3 Challenges on anisotropic reverse time migration

With increasing power of computer hardware, RTM has become one of popular industry scale processing procedures. However, the nature of RTM depends on the forward propagation and backward propagation, even in isotropic media, it requires two times computational time and memory allocation than other one-way wave equation migration algorithms. In anisotropic media, RTM requires even more space for memory allocation and large storage for storing forward wavefields (Jin et al., 2010). Comparing with other migration algorithms, although anisotropic RTM naturally takes into account both down-going and up-going waves and thus enhance

the image of steep salt flank and steeply dipping events with complex structures, the additional considerations need to spend on memory allocation and wavefield storages.

Another concern is stability condition. Although pseudo-spectral approach avoids frequency dispersion and provides dispersion-free wavefield, the application of pseudo-spectral approach on anisotropic RTM needs more computation time and memory space for Fourier Transform. Therefore, finite difference becomes regular propagator for anisotropic RTM. To avoid frequency dispersion and instability of wave propagation, additional stability condition needs to be considered. However, different anisotropic wave equations requires different stability conditions (Zhang and Zhang, 2008; Jin et al., 2010).

5.4 SUMMARY

This chapter briefly reviewed the theory governing the prestack reverse time migration in anisotropic media. Some synthetic examples validate the algorithm of anisotropic RTM compared with isotropic RTM. By taking anisotropic algorithm into account in migration schemes, the images can be substantially improved when anisotropy is present. To implement the RTM in anisotropic media, we first need to obtain the data of forward wave propagation. By propagating seismic recorded data from receivers in reversed time order, a zero-lag cross correlation imaging condition is applied to generate the partial migrated image. Stacking each partial migration images result in the final images.

The analysis of each anisotropic parameter on the image quality agrees with the conclusions of the parameter estimation by traveltime tomography. Anisotropic parameter ε represents the velocity differences between horizontal direction and vertical direction, ignoring it will simplify anisotropic media as pseudo-isotropic media. The quality of images will be significantly degraded when ignoring ε.

Parameter δ represents that how wave propagation deviates from vertical direction. In most cases δ has smaller value (Thomsen, 1986) than ε and the deviation is always small compared with the vertical velocity, therefore δ bring less influence on migration results than ε. The tilted symmetry axis controls the fast direction of wave propagations, ignoring tilted angle will result in errors on the reflector depth and dipping angles, especially on steeply dipping reflector. However, for near-flat subsurface strata, tilted symmetry axis will not spend large impact and generate acceptable results for seismic interpretation. The priorities of each anisotropic parameter agree with the error analysis of traveltime tomography. The analyses can be considered as a practical strategy for constructing anisotropic velocity model and provide potential processing steps for seismic anisotropic imaging.

CHAPTER 6: CONCLUSIONS

This dissertation has focused on the depth domain anisotropic parameter estimation and its influence on the inversion results. The analysis of anisotropy in depth domain can be found in categories: anisotropic traveltime tomography and anisotropic depth migration. The principle of each approach has been reviewed and several experiments demonstrated that the influence of anisotropy on velocity model building and seismic migration.

To conduct with anisotropic parameter estimation, the forward modeling algorithms are needed to generate synthetic data for accuracy and efficiency tests. Forward modeling schemes can be divided into two categories: ray tracing and waveform propagation. In this dissertation, shortest path ray tracing approach has been extended to incorporate with anisotropic effect. By introducing tilted angle φ of symmetry axis, the first arrivals can be directly calculated by this algorithm and considered as input data for first arrival traveltime tomography. Seismic waveform modeling has been extended from isotropy to anisotropy recently. Although waveform modeling provides several useful properties of subsurface strata, such as amplitude and phase polarity, to consider as proper anisotropic forward modeling algorithm to generate first arrivals in this dissertation, it shows low efficiency than anisotropic ray tracing. However, it is necessary for waveform tomography which is promising future research topic.

To construct anisotropic velocity model, an anisotropic layer tomography has been developed. The inversion kernels can be derived by the derivatives of TTI traveltime equation on anisotropic parameter. Each analytical kernel displays the different sensitivities of anisotropic parameter on different acquisition geometries, or incident ray angles. For example, the kernel for parameter ε reaches to a high-magnitude peak when ray angle approaches to 90°. This scenario indicates that ε is most resolvable

using ray paths around the horizontal direction, or perpendicular to the tilted symmetry axis. In contrast, the kernel for parameter δ reaches to a low-magnitude peak value around ray angle 45°, this indicates that δ can be resolved when using rays along this direction. However, the low magnitude means that it is hard to be resolved in the presence of noise. The kernel for tilted angle φ reaches to a broad peak with intermediate magnitude between ray angle 60° and 80°, indicating it has a similar sensitivity trend but less tolerant to noise in comparison with that for ε.

Layer tomography can be applied when stratigraphy is easy to identify from priory geological information. It provides less inversion variables and avoids the smearing artifacts generated by cell or grid tomography. Substituting isotropic velocity kernel with derived anisotropic kernels, the anisotropic layer tomography can be developed. In each layer, the inversion parameters can be a combination of constant anisotropic parameter ε and δ, axial velocity, tilted angle of symmetry axis or thickness-varying layers. By applying conjugate gradient scheme as inversion operator, each of anisotropic parameter can be inverted successfully. In TTI media, the inversion analysis indicates that inversion for the tilted symmetry axis of TTI models creates a new ambiguity in anisotropic seismic tomography. The error in the VTI or HTI assumptions may degrade the quality of the parameter estimation for TTI media and lead to significant distortions in the image quality.

However, inverting for five parameters together will result in nonuniqueness and make result unstable. In this dissertation, I develop a practical strategy to invert for most error-tolerant parameter; the parameter which has least error-tolerant property will be treated as last inversion parameter. The inversion of δ is particularly unstable when comparing with that for the axial velocity and ε in TTI media. However, an error in δ does not bring significant error on the inverted values of the velocity and ε. Therefore, assuming δ as zero when inverting for other parameters is a reasonable decision if no

information available about the type of the anisotropy. Although axial velocity and ε are relatively easy to invert, any gaps or deficiencies in ray path coverage could affect the resolution of the tomographic results, and the most effective solution is to use wide-azimuth data with a wide spread of sources and receivers. Even through, the choices on the complexity level of the anisotropic depth model and what parameters to invert depend on the available data quality, coverage, and study objectives.

The analysis of anisotropic parameter on prestack migration results indicates the similar trend of the importance of each parameter on the image with the priority analysis from traveltime tomography. The nature of parameter ε represents the fractional difference between horizontal velocity and vertical velocity. When assuming ε as zero for anisotropic migration, it will ignore the difference between two orthogonal velocities and treat the model as pseudo-isotropic model (δ still exists). By applying anisotropic data, the imaging quality can be seriously degraded. However, δ is used to quantify how much the direction of wave propagation deviates from vertical direction. In most cases δ has small value and it is not related with horizontal velocity, or fast velocity direction in VTI media, ignoring δ will not bring large error compared with ε. For near-flat subsurface strata, tilted symmetry axis will hardly generate large error impact on seismic interpretation. Overall, each anisotropic parameter play different role in velocity model building and depth migration. A proper method to increase anisotropic solution stability may refer to limit the size of inversion parameters resulting less underdeterminacy or perhaps assume a more restricted nature of anisotropic media, such as elliptical anisotropy.

Though a proper treatment of anisotropic estimation scheme can bring expected results, sparse and irregular data acquisition, incomplete illumination of subsurface strata and erroneous data with low signal-to-noise ratios may result in incorrect estimates especially in field data. For example, irregular acquisition can limit the range of ray

coverage and result in deficiencies in ray path direction, low signal to noise ratio will increase the difficulty and error in picking the first arrivals. Another limitation on this approach is that it is good for limited thickness-varying layers, such as less than eight or ten layers, more layers will bring more inversion variables to make whole inversion matrix underdeterminacy, which could be overcame by providing S-wave data or converted data, or move to apply seismic waveform tomography. This could be one of the promising and encouraging research topics.

REFERENCES

Alkhalifah, T., 1997, Velocity analysis using nonhyperbolic moveout in transversely isotropic media: Geophysics, 62, 1839-1854.

--------------, 1998, Acoustic approximations for processing in transversely isotropic media: Geophysics, 63, 623-631.

------------, 2000, An acoustic wave equation for anisotropic media: Geophysics, 65, 1239–1250.

Alkhalifah, T. and Tsvankin, I., 1995, Velocity analysis for transversely isotropic media: Geophysics, 60, 1550-1566.

Ball, G., 1995, Estimation of anisotropy and anisotropic 3-D prestack depth migration, offshore Zaire: Geophysics, 60, 1495-1513.

Baysal, E., D. D., Kosloff, and J.W. C., Sherwood, 1983, Reverse time migration: Geophysics, 48, 1514–1524.

Berryman, J. G., Grechka, V. Y., and Berge, P. A., 1999, Analysis of Thomsen parameters for finely layered VTI media: Geophysical Prospecting, 959-978.

Bohm, G., 2000, 3D adaptive tomography using Delaunay triangles and Voronio polygons: Geophysical Prospecting, 2000, 48, 723-744.

Cardarelli, E., and Cerreto, A., 2002, Ray tracing in elliptical media using the linear traveltime interpolation method applied to traveltime seismic tomography: Geophysical Prospecting, 50, 55-72.

Cerveny, V., 1972, Seismic rays and ray intensities in inhomogeneous anisotropic media: Geophys. JR astr. Soc., 29, 1-13.

Cerveny, V., 2001, Seismic ray theory, Cambridge University Press.

Cerveny, V., and Firbas, P., 1984, Numerical modeling and inversion of traveltime of seismic body waves in inhomogeneous anisotropic media: Geophys. J. R. Astron. Soc. 76, 41-51.

Chapman, C. and Pratt, R., 1992, Traveltime tomography in anisotropic media—I. Theory: Geophys. J. Int., 109, 1-19.

Charles S., Mitchell, D., Holt, R., Lin, J. and John, M., 2008, Data-driven tomographic velocity analysis in tilted transversely isotropic media: A 3D case history from the Canadian Foothills: Geophysics, 73, VE261-VE268.

Crampin, S., 1984, Anisotropy in exploration seismics: First Break, 19-21.

Du, X., R., Fletcher, and P. J., Fowler, 2008, A new pseudo-acoustic wave equation for VTI media: 70th Annual Conference and Exhibition, EAGE, Extended Abstracts, H033.

Duveneck, E., P. Milcik, P. M., Bakker, and C., Perkins, 2008, Acoustic VTI wave equations and their application for anisotropic reverse-time migration: 78th Annual International Meeting, SEG, Extended Abstracts, 2186–2190.

Fletcher, R. P., X., Du, and P. J., Fowler, 2009, Reverse time migration in tilted transversely isotropic (TTI) media: Geophysics, WCA179-WCA187.

Grechka, V., L., Zhang, and J. W., Rector, 2004, Shear waves in acoustic anisotropic media: Geophysics, 69, 576-582.

Hestholm, S., 2007, Acoustic VTI modeling using high-order finite-differences: 77th Annual International Meeting, SEG, Expanded Abstracts, 139–143.

Hornby, B., Schwartz, L., and John, H., 1994, Anisotropic effective-medium modeling of the elastic properties of shales: Geophysics, 59, 1570-1583.

Jiang, F., Zhou, H., Zou, Z, and H. Liu, 2009, 2D Tomographic velocity model building in tilted transversely isotropic media: 79th Annual International Meeting, SEG, Expanded Abstract, 4024-4028.

Jiang, F., and Zhou, H., 2010, A strategy to estimate anisotropic parameters by error analysis of traveltime inversion: 80th Annual International Meeting, SEG, Expanded Abstract.

Jiang, F., and Zhou, H., 2010, Traveltime inversion and error analysis for layered anisotropy: submitted to Journal of Applied Geophysics, in review.

Jin, S., Jiang, F., and Y., Ren, 2010, Comparison of isotropic, VTI and TTI reverse time migration: an experiment on BP anisotropic benchmark dataset, 80th Annual International Meeting, SEG, Expanded Abstract.

Kosloff, D., J. Sherwood, Z. Koren, E. Machet, and Y. Falkovitz, 1996, Velocity and interface depth determination by tomography of depth migrated gathers: Geophysics, 61, 1511-1523.

Klimes, L., and Kvasnicka, M., 1994, 3-D network ray tracing: Geophys, J., Int., 116, 726-738.

Kumar, C., Sen, M.K., Ferguson,, R.J., 2004, Traveltime calculation and prestack depth migration in tilted transversely isotropic media: Geophysics, 69, 37-44.

Kumar, D., Sen, M.K., Ferguson, R.J., 2008, Depth migration anisotropy analysis in the time domain: Geophysical Prospecting, 56, 87-94.

Li, P., Yan, Z., He, Y., Zhou, H., H. Liu, and F., Jiang, 2008, Application of 2D deformable layer tomostatics in western China: 78th SEG Annual Meeting, Extended Abstract, 3335-3339.

Liu, H., Zhou, H., Jiang, F., and Z., Zou, 2009a, First arrival tomography using depth varying velocity gradients, 79th Annual International Meeting, SEG, Expanded Abstract, 4034-4038.

Liu, H., Zhou, H., Zou, Z., and F., Jiang, 2009b, Improved shortest path ray tracing with locally linear velocity variations, 79th Annual International Meeting, SEG, Expanded Abstract, 2597-2601.

Musgrave, M. J. P., 1970, Crystal acoustics: Holden-Day.

Marquering, H., G., Nolet, and F. A., Dahlen, 2002, Three-dimensional waveform sensitivity kernels: Geophy., Jour., Int., 132, 521-534.

Maultzsch, S., Chapman, M., Liu, E., and X. Li, 2007, Modeling and analysis of attenuation anisotropy in multi-azimuth VSP data from the Clair field: Geophysical Prospecting, 627-642.

McMechan, G. A., 1983, Migration by extrapolation of time-dependent boundary values: Geophysical Prospecting, 31, 413–420.

Moser, T. J., 1991, Shortest path calculation of seismic rays: Geophysics, 56, 59-67.

Moser, T. J., Nolet, G., and R., Snieder, 1992, Ray bending revisited: Bull. Seis. Soc. American, 82, 259-288.

Nakanishi, I., and Yamaguchi, K., 1986, A numerical experiment on nonlinear image reconstruction from first-arrival times for two-dimensional island are structure: J. Phys. Earth, 34, 195-201.

Pratt, R. G., Shin, C., Hicks, G. J., 1998, Gauss-Newton and full Newton methods in frequency-space seismic waveform inversion: Geophysical Journal International, 133, 341-362.

Ruger, A., and Alkhalifah, T., 1996, Efficient two-dimensional anisotropic ray tracing: Seismic Anisotropy, 556-600.

Ruger, A., and Hale, D., 2006, Meshing for velocity modeling and ray tracing in complex velocity fields: Geophysics, U1-U11.

Sayers, C., 2005, Seismic anisotropy of shales: Geophysical Prospecting, 53, 667-676.

Scales, J. A., 1987, Tomographic inversion via the conjugate gradient method: Geophysics, 52,

179-185.

Sena, A., 1991, Seismic traveltime equations for azimuthally anisotropic and isotropic media: Estimation of interval elastic properties: Geophysics, 56, 2090-2101.

Shearer, P. M. and Chapman, C.H., 1988, Ray tracing in anisotropic media with a linear gradient: Geophysical Journal, 94, 575-580.

Slawinski, M. A., R. A., Slawinski, R.J., Brown, and J. M., Parkin, 2000, A generalized form of Snell's law in anisotropic media: Geophysics, 65, 632-637.

Slawinski, M. A., Lamoureux, M. P., Slawinski, R. A., and R. J., Brown, 2003, VSP traveltime inversion for anisotropy in buried layer, Geophysical Prospecting 131-139.

Thomsen, L., 1986, Weak elastic anisotropy: Geophysics, 51, 1954-1966.

Tsvankin, I., 2001, Seismic signatures and analysis of reflection data in anisotropic media: Elsevier Science Publ. Co., Inc.

Watanabe, T., Hirai, T., Sassa, K., 1996, Seismic traveltime tomography in anisotropic heterogeneous media: Journal of Applied Geophysics, 35, 133-143.

Whitmore, N. D., 1983, Iterative depth migration by backward time propagation: 53rd Annual International Meeting, SEG, Expanded Abstracts, 827–830.

Woodward, M.J., D., Nichols, O., Zdraveva, P., Whitfield, and T. John., 2008, A decade of tomography: Geophysics, 73, VE5-VE10.

Yoon, O., K., and H., Zhou, 2001, Depth imaging with multiples: Geophysics, 66, 246-255.

Zhang, H., and Y., Zhang, 2008, Reverse timemigration in 3D heterogeneousTTI media: 78thAnnual International Meeting, SEG, ExpandedAbstracts, 2196–2200.

Zhang, Y., and H., Zhang, 2009, A stable TTI reverse time migration and its implementation: 79th Annual International Meeting, SEG, Expanded Abstracts, 2794-2798.

Zhou, B., and Greenhalgh, S. A., 2005, 'Shortest path' ray tracing for most general 2D/3D anisotropic media: J. Geophys, Eng., 2, 54-63.

Zhou., B., and Greenhalgh, S., 2009, On the computation of the Frechet derivatives for seismic waveform inversion in 3D general anisotropic, heterogeneous media: Geophysics, 74, WB53-WB63.

Zhou, B., Greenhalgh, S., and Alan, G., 2008, Nonlinear traveltime inversion scheme for crosshole seismic tomography in tilted transversely isotropic media: Geophysics, 73, D17-D33.

Zhou, H., 2003, Multiscale traveltime tomography: Geophysics, 68, 1639-1649.

----------, 2006, Multiscale deformable-layer tomography: Geophysics, 71, R11-R19.

Zhou, H., Liu, H., Jiang, F., and P., Li, 2008, First-break deformable layer tomostatics constrained by shallow reflections: 78th SEG Annual Meeting, Extended Abstract, 3224-3228.

Zhou, H., G. Zhang, and R. Bloor, 2006a, An anisotropic acoustic wave equation for VTI media: 68th Annual Conference and Exhibition, EAGE, ExtendedAbstracts, H033.

----------, 2006b, An anisotropic acoustic wave equation for modeling and migration in 2D TTI media: 76th Annual International Meeting, SEG, ExpandedAbstracts, 194–198.

Zhou, R., D. McAdow, C. Barberan, D. Dushman, and Doherty, F., 2004, Seismic anisotropy estimation in TTI media using walkaway VSP data: 74th Annual International Meeting, SEG, Extended Abstract, 2525-2528.

Zou, Z., Zhou, H., Jiang, F., and H. Liu, 2009, The role of acquisition geometry and components for imaging microseismicity: 79th SEG Annual Meeting, Extended Abstract, 162-166.

APPENDIX A: THE SUBROUTINES OF CALCULATING TRAVELTIME IN TTI MEDIA

To calculate the traveltime in TTI media, Equation (2-4) is applied in shortest path ray tracing algorithm, the following shows the codes to calculate traveltime from each nodes:

From j = (0, …, number of forward nodes)

```
    {


        /*local length between tow nodes*/
         lnnew = getln_nds (ornew[j], ifwd, -1);


        /*calculating traveltime between two nodes in block jbk*/
         dtnew  =  lnnew *
                sw_tti_sin (nodes[ornew[j]].x-nodes[ifwd].x,
                          nodes[ornew[j]].z-nodes[ifwd].z,jbk);


            }


double getln_nds (ind, sd, iso) /* length between nd[ind] & nd[sd] */
int ind, sd, iso;
{ int    ix, iy;
```

```c
  if (sd>=0 && sd < mm-1)

      {

       /* source is a predefined node */

        return ( sqrtnorm2 (nodes[sd].x  -  nodes[ind].x,

                            nodes[sd].z  -  nodes[ind].z) );

      }

  else if (sd == mm-1)

      {

      /* real source */

        return ( sqrtnorm2 (nodes_sor[iso].x  -  nodes[ind].x,

                            nodes_sor[iso].z  -  nodes[ind].z) );

      }

      errmsgexit("getln_nds: sd >= mm");

}




 float sw_tti_sin (float dx, float dz, int ibk)

{

  double slowness;

  double DEL, EPS;

  double arg, sin4a, sin2a;

  int jz ;
```

```
     double dot, len, sin1, cos1;


   /* The layer which the node is located on */
jz  = ibk/NXS;


/* Distance between two nodes  */
  len = sqrt( dx * dx + dz * dz  );


   /* First, calculate sine value of incident angle */
  if (len > 0.0 )

    {
    sin1 = dx/len;

    cos1 = dz/len;

    }


  /* Calculate sin(θ-φ) */
   dot =  sin1 * cos( angle[jz] * DAR) - cos1 * sin( angle[jz] * DAR);


  /* Calculate pseudo-Pwave slowness */
  sin2a = dot * dot ;

  sin4a = sin2a * sin2a ;


  DEL = - 2.0 *  delta[jz] * sin2a ;
```

```
    EPS  =   2.0 * (delta[jz] - epsilon[jz])  * sin4a ;

   arg = 1.0 + DEL + EPS ;

   slowness = slowness[jz] * sqrt (arg);

   return (slowness) ;

 }
```

APPENDIX B: THE SUBROUTINES OF CALCULATING FRECHET TTI KERNELS

The Frechet kernels can be derived by first derivatives of Equation (2-4) on different anisotropic parameters. The index number is setup for identifying different inversion parameters, such as:

Index 1 stands for inverting for all of parameters;

Index 2 stands for inverting for layer geometry;

Index 3 stands for inverting for axial velocity;

Index 5 stands for inverting for parameter δ;

Index 7 stands for inverting for parameter ε;

Index 11 stands for inverting for tilted angle φ.

Index 2 to Index 11 can be combined arbitrarily to invert for different combinations of anisotropic parameters.

The following subroutines illustrate that how to calculate Frechet TTI kernels in traveltime tomography:

```
/* Find kernel[ray.nl] */

 ray.nl = 0;

 for(tt0=0.0, j=0; j<nry-1; j++) {

   lene = sqrtnorm2(ry[j].x - ry[j+1].x,

                    ry[j].z - ry[j+1].z);

       x = 0.5 * (ry[j].x + ry[j+1].x);

       z = 0.5 * (ry[j].z + ry[j+1].z);

     ibk = xzgetbk1_fst(x, z);

      jz = ibk/NXS;
```

```
swn0      = sw_md[jz];

delta0    = delta_md[jz] ;

epsilon0 = epsilon_md[jz] ;

angle0   = angle_md[jz];
```

/* **Calculate Analytical Kernel Expression based on Equation (3-1) to (3-4)** */

/* First, calculate sine value of incident angle*/

```
if (lene > 0.0 )

    {

    sinn = (ry[j+1].x-ry[j].x)/lene;

    cosn = (ry[j+1].z-ry[j].z)/lene;

    }


 dott =  sinn * cos(angle_md[jz] * DAR) - cosn * sin(angle_md[jz] * DAR);


  sin2a = dott * dott ;

  sin3a = sin2a * dott ;

  sin4a = sin2a * sin2a ;

  cosa = sqrt(1-sin2a);

    tga = sin(angle_md[jz] * DAR) / cos(angle_md[jz] * DAR) ;


part1 = 2 * delta0 * dott * (sinn*tga+cosn*cos(angle_md[jz] * DAR)) ;
```

```c
part2 = 4 * (epsilon0-delta0) * sin3a * (sinn*tga+cosn*cos(angle_md[jz] * DAR));


cor = sqrt( 1 - 2 * delta0 * sin2a + 2 * (delta0 - epsilon0) * sin4a ) ;


if ( index[jz]%3 == 0 )    /* invert for axial velocity*/

 {

  ker_s[ray.nl].r = lene * cor ;

  ker_s[ray.nl].i = jz * 4;

      ray.nl++;

 }


if ( index[jz]%5 == 0  )   /* invert for parameter δ*/

 {

  ker_s[ray.nl].r = (lene * swn0 * (sin4a - sin2a)) / cor ;

  ker_s[ray.nl].i = jz * 4 + 1 ;

        ray.nl++;

 }


if ( itf_var[jz]%7 == 0  )     /* invert for parameter ε */

 {

  ker_s[ray.nl].r =   (- (lene * swn0 * sin4a) / cor ) ;

  ker_s[ray.nl].i = jz * 4 + 2;

        ray.nl++;
```

```
    }


    if ( itf_var[jz]%11 == 0  )                /* invert for tilted angle φ*/

    {

    ker_s[ray.nl].r  = (lene * swn0 * (part1 + part2))/cor ;

    ker_s[ray.nl].i = jz * 4 + 3;

            ray.nl++;

    }



      sw0[j] = sw_md[jz] ;

     del0[j] = delta_md[jz];

     eps0[j] = epsilon_md[jz];

     ang0[j] = angle_md[jz];



     dt0[j] = lene * sw_tti_angle(ry[j+1].x-ry[j].x, ry[j+1].z-ry[j].z,

                      sw_md[jz], delta_md[jz], epsilon_md[jz], angle_md[jz]);

      tt0 += dt0[j];

  }
```

To calculate the layer geometry kernels, we use numerical calculation to perform:

```
    if (index[jz]%2 != 0)        continue;
```

```c
    /* perturbing the node up-down to get derivatives */

            tt0m = tt0 - dt0[j-1] - dt0[j];

            lenf =  sqrtnorm2( ry[j-1].x -  ry[j].x,

                              ry[j-1].z  - (ry[j].z + dZSEG));

            lene =  sqrtnorm2( ry[j+1].x -  ry[j].x,

                              ry[j+1].z - (ry[j].z + dZSEG));


    tt1 = tt0m + lenf * sw_tti_angle( ry[j-1].x -  ry[j].x,

                                      ry[j-1].z -( ry[j].z + dZSEG),

                          sw0[j-1],del0[j-1],eps0[j-1], ang0[j-1])    +

                lene * sw_tti_angle( ry[j+1].x -  ry[j].x,

                                     ry[j+1].z - (ry[j].z+dZSEG),

                          sw0[j],del0[j],eps0[j], ang0[j]);


      if (tt1 == tt0)          continue;


    dtdz = (tt1 - tt0) / (double)dZSEG;


  float sw_tti_angle (float dx, float dz, float swn,float delta4, float epsilon4, float angle4)

  {

    double slowness;

    double DEL, EPS, dot;

    double arg, sin2a, sin4a, sin1, cos1;
```

```
      float len ;


      len = sqrt( dx * dx + dz * dz  );


   if (len > 0.0 )

        {

         sin1 = dx/len;

        cos1 = dz/len;

         }

          dot =  sin1 * cos(angle4 * DAR) - cos1 * sin(angle4 * DAR);


    sin2a = dot * dot ;

    sin4a = sin2a * sin2a ;

    DEL = - 2.0 * delta4 * sin2a ;

    EPS = 2.0 * (delta4 - epsilon4)  * sin4a ;

    arg = 1.0 + DEL + EPS ;

    slowness = swn * sqrt (arg);

    return (slowness) ;

}
```